# MONTE CARLO SHIELDING ANALYSIS CAPABILITIES WITH MAVRIC

RADIATION PROTECTION

**KEYWORDS:** *Monte Carlo, variance reduction, shielding*

DOUGLAS E. PEPLOW*

*Oak Ridge National Laboratory, Nuclear Science and Technology Division*
*P.O. Box 2008, Building 5700, Oak Ridge, Tennessee 37831-6170*

Received July 1, 2009
Accepted for Publication May 25, 2010

*Monte Carlo shielding analysis capabilities in SCALE 6 are centered on the Consistent Adjoint Driven Importance Sampling (CADIS) methodology. CADIS is used to create an importance map for space/energy weight windows as well as a biased source distribution. New to SCALE 6 are the Monaco functional module, a multigroup fixed-source Monte Carlo transport code, and the Monaco with Automated Variance Reduction using Importance Calculations (MAVRIC) sequence. MAVRIC uses the Denovo code (also new to SCALE 6) to compute coarse-mesh discrete ordinates solutions that are used by CADIS to form an importance map and biased source distribution for the Monaco Monte Carlo code. MAVRIC allows the user to optimize the Monaco calculation for a specific tally using the CADIS method with little extra input compared with a standard Monte Carlo calculation. When computing several tallies at once or a mesh tally over a large volume of space, an extension of the CADIS method called FW-CADIS can be used to help the Monte Carlo simulation spread particles over phase space to obtain more uniform relative uncertainties.*

## I. INTRODUCTION

The application of Monte Carlo transport methods to deep penetration shielding problems requires variance reduction in order to obtain statistically meaningful results within reasonable periods of time. With the correct variance reduction, the Monte Carlo code can spend more time tracking particles that contribute to the various tallies while spending less time on particles that do not. Applying traditional methods of variance reduction can be quite time consuming for the user and requires a great deal of experience to ensure that the final answers have not been incorrectly biased. For a long time there have been codes that use approximate adjoint discrete ordinates calculations as the basis for variance reduction, in both space and energy, in Monte Carlo calculations [e.g., AVATAR (Ref. 1), SAS4 (Ref. 2), ADVANTG (Ref. 3)]. Recent work has also shown how this type of variance reduction can be performed automatically by the computer—based on the user's original Monte Carlo input and a description of what the user wishes to optimize. The result is a hybrid method, which obtains better performance out of a Monte Carlo simulation by using information from a discrete ordinates calculation.

The new shielding analysis tools in SCALE 6 have been designed with this type of advanced variance reduction method in mind. The Monaco with Automated Variance Reduction using Importance Calculations (MAVRIC) sequence performs radiation transport on problems that are too challenging for standard, unbiased Monte Carlo methods. MAVRIC is based on the Consistent Adjoint Driven Importance Sampling (CADIS) methodology, which uses an importance map and biased source that are derived to work together. MAVRIC automatically performs a coarse-mesh, three-dimensional (3-D), discrete ordinates calculation using the new Denovo $S_N$ code to determine the adjoint flux as a function of position and energy. This adjoint flux information is then used by MAVRIC to construct a space- and energy-dependent importance map (i.e., weight windows) to be used for biasing during particle transport and a mesh-based biased source distribution. MAVRIC then passes the importance map and biased source distribution to the Monte Carlo transport code Monaco.

*E-mail: peplowde@ornl.gov

## II. THE MONACO FUNCTIONAL MODULE

Monaco is a general purpose, 3-D, fixed-source, multigroup Monte Carlo shielding code that uses the SCALE General Geometry Package (SGGP), the same as used by the criticality code KENO-VI, and cross-section files produced by the standard SCALE material information processor. Monaco was originally based on the MORSE Monte Carlo code but has been extensively modified to modernize the coding; to incorporate more capability in terms of sources, tallies, and variance reduction; and to read a user-friendly block/keyword style input.

### II.A. Source Descriptions

The source description for a Monaco calculation is specified by its total strength and three separable distributions: spatial, energy, and directional.

#### *II.A.1. Spatial Distribution*

The spatial distribution is simple but very flexible—the source is treated as uniform over a given solid shape defined in global coordinates, optionally limited by the underlying SGGP geometry variables of unit, media, and mixture. In this way, source volumes (or planes, lines, or points) can be defined that are independent of or dependent on the model geometry. A cylinder or cylindrical shell can be oriented with its axis in any direction. The basic solid shapes and their allowed degenerate cases are listed in Table I.

Monaco samples the source position uniformly over the basic solid and then uses rejection if any of the optional SGGP geometry limiters have been specified. For sources that are confined to a particular unit, media, or mixture, users should try to ensure that the basic solid containing the source tightly bounds the desired region for efficient sampling.

#### *II.A.2. Energy Distribution*

The energy distribution of the source is a simple, binned distribution over the groups defined by the user's choice of cross-section library. The distribution is normalized by Monaco, and the sampled source energy group is simply selected from the distribution. For example, if the cross-section library has a total of $G$ groups, the user can specify the total number of source particles for each group $S_g$, where

$$S = \sum_g S_g \ , \tag{1}$$

and the normalized distribution describing the true source is then

$$t_g = S_g / S \ , \tag{2}$$

with a total source strength of $S$. Since the source distribution is normalized by Monaco, the user needs only to supply the total source strength.

The sampled source energy group can be biased in Monaco in either of two ways: by specifying a biased distribution from which to actually sample or by specifying the importances for each group, which are then used to form the biased distribution. For the first method, the user specifies the true source distribution $S_g$ and the distribution from which to sample $A_g$. Monaco will normalize each, forming the true distribution $t_g$ and the biased distribution $a_g$:

$$a_g = A_g \Big/ \sum_g A_g \ . \tag{3}$$

For the second method, the user specifies the true source distribution $S_g$ and the importance of each group, $I_g$. Monaco will normalize the true distribution to form $t_g$ and then compute the biased distribution as

$$a_g = t_g I_g \Big/ \sum_g t_g I_g \ . \tag{4}$$

Either way, Monaco will sample source particles from the biased distribution $a_g$ and assign the starting weight $w_0$ as the ratio of the true probability of the sampled group to the biased probability of the sampled group:

$$w_0 = t_g / a_g \ . \tag{5}$$

#### *II.A.3. Directional Distribution*

In a similar manner as the energy distribution, the directional distribution of the source particles can be specified by the user and can optionally be biased. The true distribution is specified by the amounts in each directional bin, the number and boundaries of which are determined by the user and are listed in terms of the cosine of the polar angle with respect to some reference direction in global coordinates. Biasing can be done in two ways, by specifying either the biased directional distribution or the importances for each directional bin.

TABLE I

Available Source Shapes and Their Allowed Degenerate Cases

| Shape | Allowable Degenerate Cases |
|---|---|
| Cuboid | Rectangular plane, line, point |
| Cylinder | Circular plane, line, point |
| Cylindrical shell | Cylinder, planar annulus, circular plane, cylindrical surface, line, ring, point |
| Sphere | Point |
| Spherical shell | Sphere, spherical surface, point |

If no directional distribution is specified, the default is an isotropic distribution (one directional bin from $\mu = -1$ to $\mu = 1$). The default reference direction is the positive $z$-axis ($\langle 0,0,1 \rangle$).

*II.A.4. Mesh Source Map Files*

As an alternative to specifying the separate spatial and energy distributions, a Monaco mesh source file can be used. A mesh source consists of a 3-D Cartesian mesh that overlies the physical geometry. Each mesh cell has some probability of emitting a source particle, and within each mesh cell a different energy distribution can be sampled. The position within each mesh cell is sampled uniformly, and the emission direction is sampled from the directional distribution (as described earlier), if it is given. The position within the cell can be limited by the physical geometry by specifying to keep source particles only in a certain unit, media, or mixture. Mesh source files can contain biasing information, both spatial and energy. Monaco mesh source files are produced by the MAVRIC sequence when it creates the mesh-based importance map.

### II.B. Tallies

Monaco allows three tally types: point detectors, region tallies, and mesh tallies. Each is useful in determining quantities of interest in the simulation. Any number of each can be used, up to the limit of machine memory. The tallies compute flux for each group, the total neutron and total photon fluxes, and any number of dose or dose-like responses. A typical dose-like response $R$ is the integral over all energy groups of the product of a response function $f_g$ and the group flux $\phi_g$:

$$R = \sum_g f_g \phi_g \quad . \tag{6}$$

Monaco tallies are really just collections of simple tallies for each group, the total flux, each group contribution to a response, and the total response. The simple tally works in the following way: a history score $h_i$ is zeroed out at the start of each history. During the course of the history $i$, when an event occurs during substep $j$, a score consisting of some contribution $c_{ij}$ weighted by the current particle weight $w_{ij}$ is calculated and added to the history score $h_i$. At the end of the history, the history score is the total weighted score for each substep $j$ in the history:

$$h_i = \sum_j w_{ij} c_{ij} \quad . \tag{7}$$

Note that the value for the contribution $c_{ij}$ and the point when it is added to the accumulator are determined by the tally type. At the end of each history, the history score is added to two accumulators, the first for finding the tally average $a$ and the second for finding the uncertainty in the tally average, $b$:

$$a = \sum_i h_i \tag{8}$$

and

$$b = \sum_i h_i^2 \quad . \tag{9}$$

At the end of all $N$ histories, the tally average $\bar{x}$ and uncertainty in the tally average $u$ are found using

$$\bar{x} = \frac{1}{N} a \tag{10}$$

and

$$u^2 = \frac{1}{N} \left( \frac{1}{N} b - \bar{x}^2 \right) \quad . \tag{11}$$

The tally average and uncertainty can then be scaled with multiplicative constants or units conversions.

Simulations are divided into batches (10 to 100) of histories where at the end of each batch, detailed, group-by-group results for each tally are saved to separate files. Users can view these files as the Monaco simulation progresses. The batching and batch size do not affect the statistics of the tallies—only the total number of histories simulated matter. Summaries of the tallies appear in the final Monaco output file.

*II.B.1. Point Detector Tallies*

Point detector tallies use a form of variance reduction in computing the flux or response at a specific point. At the source emission site and at every interaction in the particle's history, an estimate is made of the probability that the particle will strike the position of the point detector. For each point detector, Monaco tallies the uncollided and total flux for each energy group, the total for all neutron groups, and the total for all photon groups. Any optional dose-like responses are calculated as well.

After a source particle of group $g$ is started, the distance $R$ between the source position and the detector position is calculated. Along the line connecting the source and detector positions, the sum of the distance $s_j$ through each region $j$ multiplied by the total cross section $\sigma_j^g$ for that region is also calculated. The contribution $c_g$ to the uncollided flux estimator is then made to the tally for group $g$:

$$c_g = \frac{1}{4\pi R^2} \exp\left( -\sum_j s_j \sigma_j^g \right) \quad . \tag{12}$$

At each interaction point during the life of the particle, similar contributions are made to estimate the collided flux to the tallies. For each group $g'$ that the particle could scatter into and that could reach the detector location, a contribution is made that also includes the probability to scatter from group $g$ to group $g'$.

This type of tally is costly since ray-tracing through the geometry from the particle position to the detector location is required many times over the particle history. Point detectors can be located only in regions made of void material, so that contributions from interactions arbitrarily close to the point detector cannot overwhelm the total estimated flux.

Care must be taken in using point detectors in deep penetration problems to ensure that the entire phase space that could contribute has been well sampled—so that the point detector is not underestimating the flux by leaving out areas far from the source but close to the point detector position. One way to check this is by examining how the tally average and uncertainty change with each batch of particles used in the simulation. Large fluctuations in either quantity could indicate that the phase space is not being sampled well.

Each point detector tally will create a text file for the final detailed group-by-group results. Each tally also creates a *.chart file that records the total neutron flux, the total photon flux, and the total response function value after each batch completes. This second file can be displayed using the Interactive Plotter, a Java utility shipped with SCALE 6, to look at the convergence behavior of the tally.

### *II.B.2. Region Tallies*

Region tallies are used for calculating the flux or responses over one of the regions listed in the SGGP geometry. Both the track-length estimate and the collision density estimate of the flux are calculated; for each, the region tally contains simple tallies for finding the flux in each group, the total neutron flux, and the total photon flux. For each of the optional response functions, the region tally also contains simple tallies for each group and the total response.

For the track-length estimate of flux, each time a particle of energy group $g$ moves through the region of interest, a contribution of $l$ (the length of the step in the region) is made to the history score for the simple tally for flux for group $g$. The same contribution is made for the history score for the simple tally for total particle flux, neutron or photon, depending on the particle type.

If any optional response functions were requested with the tally, then the contribution of $lf_g$ is made for the response group, where $f_g$ is the response function value for group $g$. The history score for the total response function is also incremented using $lf_g$.

At the end of all of the histories, the averages and uncertainties of all of the simple tallies for fluxes are determined for every group and each total. These results then represent the average track length over the region. To determine flux, these are divided by the volume of the region. If the volume $V$ of the region was not given in the geometry input nor calculated by Monaco, then the tally results are just the average track lengths and their uncertainties. A reminder message is written to the tally detail file if the volume of the region was not set.

For the collision density estimate of the flux, each time a particle of energy group $g$ has a collision in the region of interest, a contribution of $1/\sigma_g$ (the reciprocal of the total cross section of group $g$) is made to the history scores for the simple tally for flux for group $g$ and for the total particle flux. At the end of the simulation, the averages and uncertainties of all of the simple tallies for every group flux and total flux are found and then divided by the region volume, if available.

In a manner similar to the point detector tallies, region tallies also produce text files listing the tally average and uncertainty at the end of each batch of source particles, as well as the final group-by-group results of the fluxes and any responses.

### *II.B.3. Mesh Tallies*

For a 3-D Cartesian mesh overlying the SGGP geometry, Monaco can calculate the track-length estimate of the flux. Since the number of cells (voxels) in a mesh can become quite large, the mesh tallies are not updated at the end of each history but are instead updated at the end of each batch of particles. This prevents the mesh tally accumulation from taking too much time but means that the estimate of the statistical uncertainty is slightly low.

Mesh tallies can calculate optional response functions also. A response function value $R(x, y, z)$ is simply the integral of the product of the group fluxes in each cell $\phi_g(x, y, z)$ with each response function $f_g$:

$$R(x, y, z) = \sum_g f_g \phi_g(x, y, z) \ . \tag{13}$$

Because of the large sizes of mesh tallies, the responses are calculated only when the final mesh tally is saved. The uncertainties $\sigma_R(x, y, z)$ reported for the response function values are estimated as

$$\sigma_R(x, y, z) = \sqrt{\sum_g f_g^2 \sigma_{\varphi, g}^2(x, y, z)} \ . \tag{14}$$

Mesh tallies can be viewed with the Mesh File Viewer, a Java utility that can be run from GeeWiz (on PC systems), or can be run separately on any type of system. The Mesh File Viewer will show the flux for each group, the total flux for each type of particle, and the optional responses. Uncertainties and relative uncertainties can also be shown for mesh tallies using the Mesh File Viewer. More detailed information on the Mesh File Viewer is contained in its online documentation.

## II.C. Conventional Biasing

Similar to other Monte Carlo codes, Monaco offers a few of the conventional biasing methods. Like source energy and direction biasing, these biasing methods typically require some knowledge about what the ultimate

solution will look like and may require some iteration to get the best parameters.

*II.C.1. Forced Collisions*

Forced collisions are one of the simplest variance reduction techniques. This method forces a particle to have a collision somewhere along its current flight direction before leaving the geometry. Because the collision is forced, the particle weight is reduced by the true probability of having a collision within the geometry. This is helpful in small or low-density geometries in which many particles leave without interacting, but it can add computation time to ordinary problems. The use of forced collisions requires the use of Russian roulette (see Sec. II.C.3).

*II.C.2. Path-Length Stretching*

Path-length stretching allows particles going a certain direction to travel farther (with reduced weight) before interacting. The direction for stretching can be one of the coordinate axis directions (in global or local space), can be cylindrically or spherically outward from the origin, or can be toward some user-defined location. The amount of stretching is specified for each energy group and region.

*II.C.3. Weight Windows*

Monaco can use Russian roulette to prevent low particle weights from being tracked and splitting to prevent the production of high-weight particles. Weight windows is one way that Russian roulette and splitting can be used together to reduce the variance in the weights of the particles traveling through a given region of phase space. Monaco allows the user to specify the target weight $\bar{w}$, the lower weight $l$, used for roulette, and the upper weight $u$, used for splitting for every energy group in every geometrical region. Users can alternatively just specify the target weights and a window ratio. The window ratio $r$ is the ratio of the upper weight window to the lower weight window. So, given a target weight and a window ratio, the lower and upper weights can be found as

$$l = \bar{w}\,\frac{2}{r+1} \tag{15}$$

and

$$u = \bar{w}\,\frac{2r}{r+1}\ . \tag{16}$$

The particle weight is checked after every collision. For region-based weight windows, the particle weight is checked at each region crossing. For the mesh-based weight windows, the weight is checked every time the particle crosses a mesh boundary.

A target weight of 0 will prevent particles of that energy group in that region from being transported. For example, to perform a neutron-only calculation using a coupled neutron-photon library, the target weight values for all of the photon groups in every region can be set to 0. The user should be careful not to "turn off" energy groups or regions that may impact (bias incorrectly) the final tally results.

Monaco always uses the implicit capture technique—at collision sites, absorption is not simulated but instead the particle weight is reduced by the ratio of the scatter probability to the total interaction probability. Particles stop only if they escape the defined geometry. This technique generally produces tally results with lower uncertainties in less time, but for highly scattering or very large geometries, particles with very low weights will be tracked until their weights reach the lower limit of real numbers in double precision. This is not typically what the user wants. So, for problems that do not use any other variance reduction methods, Russian roulette should be used to prevent Monaco from following extremely low-weight particles.

*II.C.4. Mesh-Based Importance Map*

The user can alternatively specify an existing Monaco mesh-based importance map—a binary file containing the target weight for every energy group and every cell of a 3-D Cartesian mesh that overlies the physical geometry. With these target weights, the user also specifies a weight window ratio. Mesh-based importance map files are produced by the MAVRIC sequence at the same time it produces the mesh-based biased source distribution.

For effective use of an importance map, the source should be biased to match. If particles leave the importance map but are still in the defined geometry, the simulation will be stopped.

### II.D. Monaco Validation

Included with the release of SCALE 6 are three new coupled neutron-photon cross-section libraries. ENDV/B-VII.0 data were used to make a fine-group (200 neutron and 47 photon) library and a coarse-group (27 neutron and 19 photon) library. A fine-group library was also made using ENDF/B-VI.8 data. The fine-group structure is similar to the VITAMIN groups but with the highest neutron group extended to 20 MeV. As part of the validation of these new libraries and the new Monaco and MAVRIC codes, several comparisons to simple benchmark measurements were made, which are summarized below. Other comparisons between Monaco and MAVRIC and the older SAS4 sequence were also made using older cross-section libraries.[4]

*II.D.1. Neutron Transmission Through an Iron Sphere*

In the early 1990s, several experimental measurements were performed in order to benchmark ENDF/

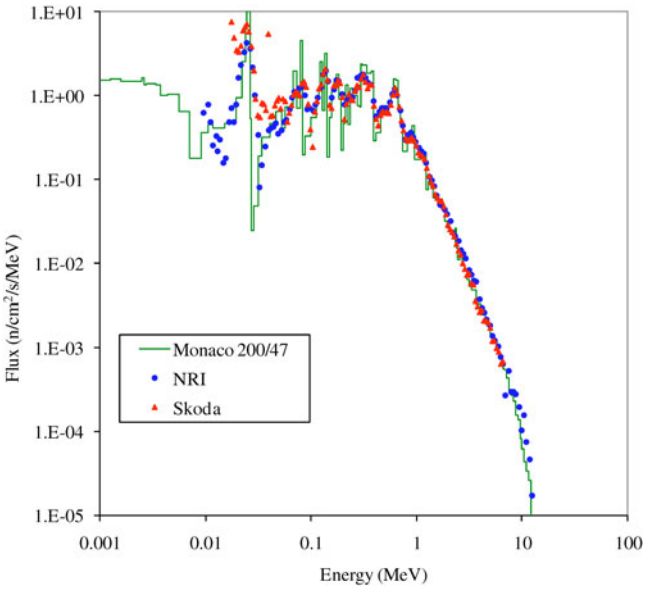


Fig. 1. Energy-dependent flux from $^{252}$Cf neutrons passing through an iron sphere; Monaco results compared with two sets of experimental measurements.

B-VI cross-section data for iron.[5] The transmission of $^{252}$Cf neutrons through a sphere of iron was measured by two teams—the Czechoslovakian National Research Institute (NRI) and the Skoda Company. The experiment was modeled in Monaco with a point source, emitting a Watt spectrum of neutrons, at the center of an iron spherical shell ($r_{in} = 1.25$ cm and $r_{out} = 25.0$ cm). The detector was 1 m from the center of the sphere. The published experimental results were normalized so that the total flux at the detector without the shield would have been 1 n/cm$^2 \cdot$s$^{-1}$. Relative errors for each measured energy bin varied from a few percent for the 500-keV range to very large values (20 to 40%) at mega-electron-volt neutron energies.

Monaco and the ENDF/B-VII.0 library were used to calculate the energy-dependent flux at 1 m using all three types of Monaco tallies—a region tally (thin shell at 1 m), a point detector, and a mesh tally. Point detector tally relative uncertainties for each energy group were typically $<2\%$. Region tally relative uncertainties were typically $<5\%$. The results of these tallies agreed well with the experimental measurements, considering some of the large uncertainties in the measured data. The region tally and the data from the experiments are shown in Fig. 1.

### *II.D.2. Neutrons Through a Heavy Water Sphere*

The transmission of $^{252}$Cf neutrons through a sphere filled with heavy water was measured in Prague in the mid-1990s (Ref. 6). For each experiment, two measurements were made, one with an iron/polyethylene shield and one without the shield. These two measurements were subtracted to account for scatter from the floor (which is about a 5% effect for energies above 10 keV). A great amount of detail is given in Ref. 6 for the materials and geometry of the source holder, insertion tube, and detectors. Two different assemblies holding the californium source were measured. Experimental uncertainties ranged from $<1$ to 30%.

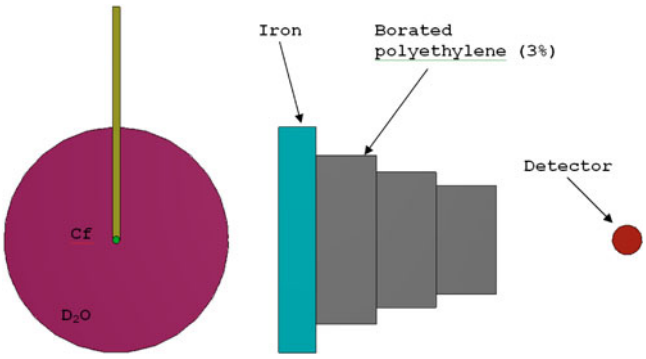


Fig. 2. Geometry model of the heavy water sphere measurement.

The Monaco calculations included the basics of the experiment. The geometry is shown in Fig. 2 for the case in which the iron/polyethylene shield is in place. Also included in the model were the concrete walls of the $10 \times 13 \times 25$ m experimental hall. The source was modeled as a small spherical source emitting a Watt spectrum of neutrons into the 30-cm-diam tank of heavy water. Monaco collected the energy-dependent flux using a point detector tally 75 cm from the center of the heavy water sphere. The relative uncertainties in most energy bins were $<2\%$. The ENDF/B-VII.0 cross-section library was used. The results matched the experimental measurements well (considering experimental uncertainties), as shown in Fig. 3.

### *II.D.3. Neutron and Photon Leakage Spectra Through Iron Spheres*

Neutron and photon leakage spectra were measured from a $^{252}$Cf source through iron spheres of various diameters in Russia during the 1980s (Ref. 7). Seven sets of experimental data for neutron leakage were presented in this benchmark, one for the bare source and one for each of six different diameters of iron shielding of 20, 30, 40, 50, 60, and 70 cm. Six sets of data were presented for photons—bare and 30-, 40-, 50-, 60- and 70-cm sphere diameters. Each data set was the difference of two measurements, one with and one without a cone-shaped shield between the source and detector. The geometry model is shown in Fig. 4.

Monaco and the new ENDF/B-VII.0 200n/47g shielding library were used to compute leakage spectra of both neutrons and photons according to the benchmark instructions. For the Monaco neutron source, the

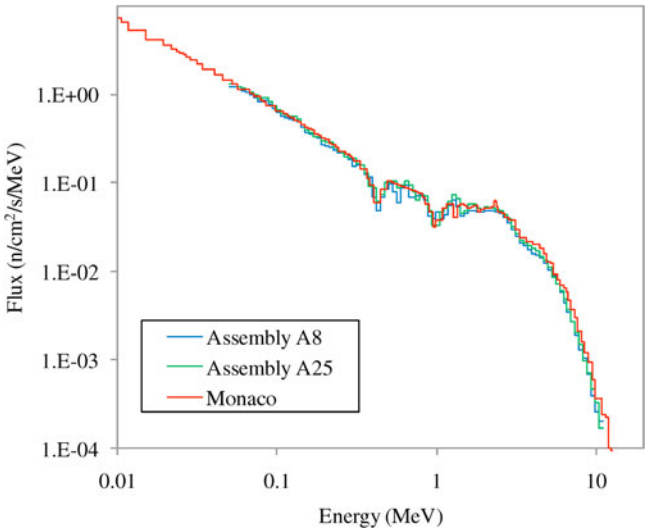


Fig. 3. Energy-dependent flux from $^{252}$Cf neutrons passing through a $D_2O$ sphere; Monaco results compared with experimental measurements from two source assemblies.

experimentally measured neutron flux spectrum of the bare source was converted into a 200-group source specification. For the Monaco photon source, the experimentally measured photon flux spectrum of the bare source was converted into a 47-group source specification. Note that the "bare source" did include copper and steel canisters, so a small fraction of the measured photon flux could have come from secondary gammas from neutrons interacting in the source capsule. For every neutron emitted from the $^{252}$Cf source, 3.82 photons were emitted. Monaco combined the sources into a single coupled neutron/photon source.

The Monaco-computed neutron fluxes agreed with the measurements, as shown in Fig. 5. The benchmark results listed in Ref. 7 are in terms of $4\pi R^2\Phi(E)/Q$, where $R$ is the radius of the detector (three times the radius of the shield, or 60 cm for the bare source) and $Q$ is the neutron source strength. Experimental uncertainties ranged from 5 to 30%, so the experimental values are shown on the plots as two lines, representing the values $\pm 1\sigma$. Photon fluxes at the detector computed by Monaco were substantially below the measured values but did compare well to MCNP5 calculations,[8] as shown in Fig. 6.

## III. OPTIMIZING THE CALCULATION OF A SINGLE TALLY

MAVRIC is an implementation of CADIS using the Denovo (Ref. 9) $S_N$ and the Monaco Monte Carlo functional modules. Source biasing and a mesh-based importance map, overlying the physical geometry, are the basic methods of variance reduction. To make the best use of an importance map, the map must be made consistent with the source biasing. If the source biasing is inconsistent with the weight windows that will be used during the transport process, source particles will undergo Russian roulette or splitting immediately, wasting computational time and negating some of the intention of the biasing. CADIS has already been well described in the literature,[3,10–12] so only a brief overview is given here.

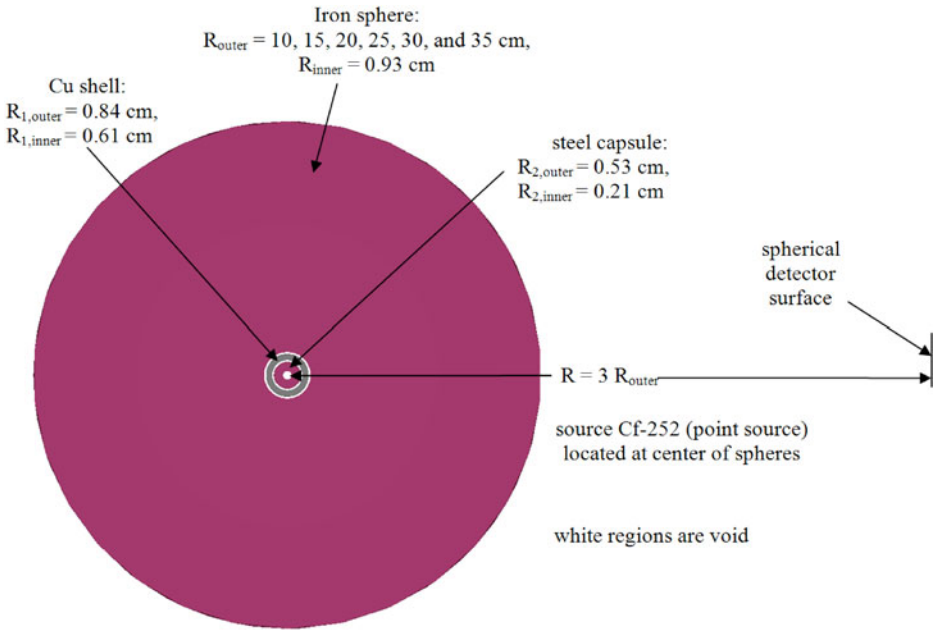


Fig. 4. Geometry model of the iron sphere measurement, without the shield.

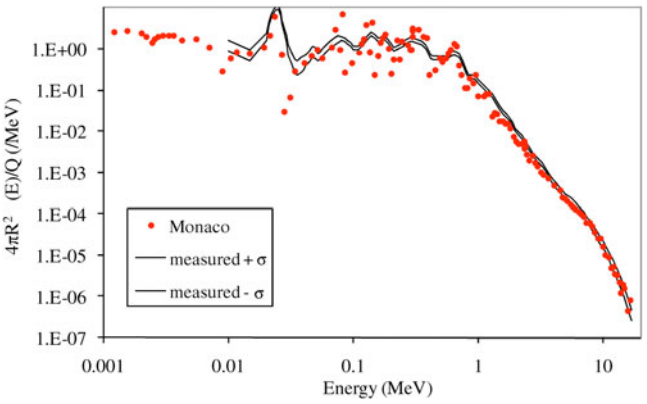


Fig. 5. Comparison of the neutron calculation with the measurement of the 70-cm shield.

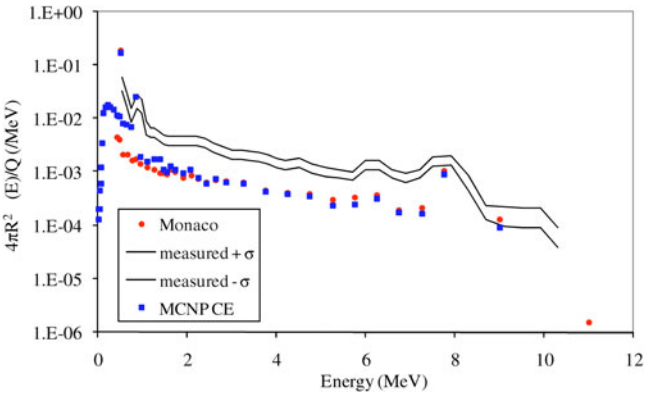


Fig. 6. Photon flux through the 70-cm shield as calculated by Monaco and MCNP5.

### III.A. Methods/Implementation

Consider a classical source-detector problem described by a unit source with emission probability distribution function $q(\vec{r},E)$ and a detector response function $\sigma_d(\vec{r},E)$. To determine the total detector response $R$, the forward scalar flux $\phi(\vec{r},E)$ over the detector volume $V_D$ must be known. The response is found by integrating the product of the detector response function and the flux over the detector volume:

$$R = \int_E \int_{V_D} \sigma_d(\vec{r},E)\,\phi(\vec{r},E)\,dV\,dE \quad . \tag{17}$$

Alternatively, if the adjoint scalar flux $\phi^+(\vec{r},E)$ is known from the corresponding adjoint problem with adjoint source $q^+(\vec{r},E) = \sigma_d(\vec{r},E)$, then the total detector response could be found by integrating the product of the forward source and the adjoint flux over the source volume $V_S$:

$$R = \int_E \int_{V_S} q(\vec{r},E)\,\phi^+(\vec{r},E)\,dV\,dE \quad . \tag{18}$$

Unfortunately, the exact adjoint flux may be just as difficult to determine as the forward flux. But, an approximation of the adjoint flux can still be used to form an importance map and a biased source distribution for use in the forward Monte Carlo calculation.

#### *III.A.1. Adjoint-Driven Importance Sampling*

The Monte Carlo solution to a source-detector problem has been shown to be best optimized by using weight windows that are inversely proportional to an adjoint flux that was the result of an adjoint calculation using the detector response function as the adjoint source. Such an importance map will minimize the variance in the forward Monte Carlo calculation of $R$ (Ref. 12). Given a detector response function $\sigma_d(\vec{r},E)$—which is a set of flux-to-dose conversion factors, a material cross section for determining reaction rates, or a detector count rate per unit flux, etc.—an adjoint problem is developed using adjoint source $q^+(\vec{r},E)$ equal to that response function:

$$q^+(\vec{r},E) = \sigma_d(\vec{r},E) \quad . \tag{19}$$

Weight window target values, $\overline{w}(\vec{r},E)$, are constructed to be inversely proportional to the resulting adjoint fluxes $\phi^+(\vec{r},E)$ as

$$\overline{w}(\vec{r},E) = \frac{c}{\phi^+(\vec{r},E)} \quad , \tag{20}$$

where $c$ is a constant.

#### *III.A.2. Consistent Biased Source*

A biased source distribution can be developed to work with the weight windows so that particles are not split or rouletted right after their birth, wasting computer time. For consistency between the forward source $q(\vec{r},E)$ and the weight windows, a biased source $\hat{q}(\vec{r},E)$ should be constructed so that source particles are born with starting weights $w_0(\vec{r},E)$ matching the weight windows of the position and energy group into which they are born. Starting weight is defined as the ratio of the true probability of the source particle just sampled to the biased probability of that source particle:

$$w_0(\vec{r},E) \equiv \frac{q(\vec{r},E)}{\hat{q}(\vec{r},E)} \quad . \tag{21}$$

To make the starting weights equal to the weight window targets, the biased source $\hat{q}(\vec{r},E)$ should be

$$\hat{q}(\vec{r},E) = \frac{q(\vec{r},E)}{\overline{w}(\vec{r},E)} = \frac{1}{c}\, q(\vec{r},E)\phi^{+}(\vec{r},E) \ , \qquad (22)$$

where the constant $c$ is determined so that the biased source distribution is a probability distribution function—it must integrate to 1,

$$\iint \hat{q}(\vec{r},E)\, d\vec{r}\, dE = 1 \ , \qquad (23)$$

giving $c$ a value of

$$c = \iint q(\vec{r},E)\phi^{+}(\vec{r},E)\, d\vec{r}\, dE \ , \qquad (24)$$

which (using adjoint theory) is equivalent to

$$c = \iint \sigma_d(\vec{r},E)\phi(\vec{r},E)\, d\vec{r}\, dE \ , \qquad (25)$$

which is equal to the overall response $R$ that was to be optimized.

This is the "consistent" part of CADIS—source particles are born with a weight matching the weight window of the region/energy into which they are born. The source biasing and the weight windows work together.

### *III.A.3. Implementation of CADIS in MAVRIC*

The first step in implementing CADIS in MAVRIC is to define the adjoint source, both its spatial component and its energy component. The spatial component is usually a point or volume where a specific tally is located, and the energy component is typically the specific response $\sigma_d(E)$ to optimize [or $\sigma_d(E) = 1$ to optimize total flux] for that tally. MAVRIC creates an input file for the Denovo $S_N$ code for this adjoint problem. Denovo returns the scalar adjoint fluxes $\phi^{+}(\vec{r},E)$ to MAVRIC on a 3-D Cartesian mesh. When constructing the mesh to use for the discrete ordinates, users should also select mesh planes around and through the source so that this mesh-based version of the source will be an accurate representation.

The next step is to create a mesh-based representation of the true source distribution on the same space/energy mesh as the adjoint fluxes. MAVRIC does this by determining what fraction of each mesh cell is contained within the defined source by testing points uniformly within each voxel. For very small or degenerate sources (points, lines, planes), a number of source points are sampled to see which voxel they are born into.

Then, an estimate of the overall response $R$ for the tally is made:

$$R = \iint q(\vec{r},E)\phi^{+}(\vec{r},E)\, d\vec{r}\, dE \ ; \qquad (26)$$

the weight window target values are computed:

$$\overline{w}(\vec{r},E) = \frac{R}{\phi^{+}(\vec{r},E)} \ ; \qquad (27)$$

and the consistent biased source distribution is formed:

$$\hat{q}(\vec{r},E) = \frac{1}{R}\, q(\vec{r},E)\phi^{+}(\vec{r},E) \ . \qquad (28)$$

Both the target weights and the biased source are stored as mesh-based quantities, using the same mesh and energy structure as the scalar adjoint flux data. The weight windows and biased source distribution are passed to the Monaco functional module and work together to sample more Monte Carlo particles in the portion of phase space most important to the specific response used as the adjoint source. In effect, particles are pushed toward the adjoint source at the expense of other parts of phase space.

### *III.A.4. Using the MAVRIC Sequence*

To use MAVRIC with the CADIS advanced variance reduction, the user specifies all of the typical input required for a standard Monte Carlo calculation (geometry, materials, source, tallies, etc.) and supplies two extra items: a description of the adjoint source to use (typically similar to one of the tallies) and the geometric mesh to use for the adjoint calculation, weight windows, and biased source. All of the CADIS calculations and the preparation of the final Monaco input are automated. Running a MAVRIC calculation using CADIS requires little extra effort on the part of the user—especially compared with the iterative process of trying to guess region-based weight windows through many forward Monte Carlo runs.

Constructing the coarse mesh to use in the importance calculations does not need to be as detailed as a stand-alone discrete ordinates calculation, but it should be representative of the problem. In MAVRIC, the goal is to use the $S_N$ calculation for a quick estimate. Accuracy is not paramount—an approximation of the overall shape of the true importance map will help the forward Monte Carlo calculation. However, the more accurate the importance map, the more efficient the forward Monte Carlo will be. At some point there is a time trade-off such that calculating the importance map requires more effort than is required by a standard analog calculation. Small mesh sizes (or large numbers of mesh cells) for $S_N$ calculations also use a great deal of computer memory.

So in MAVRIC, mesh cell sizes can be larger than what most $S_N$ practioners would use to keep the memory requirement down and the run time short. Some general guidelines to keep in mind when creating a mesh for the importance map/biased source are as follows:

1. The true source regions should be included in the mesh with mesh planes at their boundaries.

2. Point or very small sources should be placed in the center of a mesh cell, not on a mesh plane.

3. Any locations in the geometry from which particles could eventually contribute to the tallies (the "important" areas) should be included in the mesh.

4. Point adjoint sources (corresponding to point detector locations) do not have to be included in the mesh. If they are included in the mesh, they should be located at a mesh cell center, not on any of the mesh planes.

5. Volumetric adjoint sources should be included in the mesh with mesh planes at their boundaries.

6. Mesh planes should be placed at significant material boundaries.

7. Neighboring cell sizes should not be drastically different.

8. Smaller cell sizes should be used where the adjoint flux has large spatial changes, for example, near the surfaces of adjoint sources and shields (rather than within their interiors).

The default values for the various calculational parameters and settings used by Denovo for the MAVRIC sequence should cover most applications. These settings can be changed by the interested user. The two most basic parameters required by the discrete ordinates calculation are the quadrature set and the number of the Legendre polynomials used in describing the angular scattering. The default quadrature order that MAVRIC uses is $S_8$, and for the number of Legendre polynomials, the default is $P_3$ (or the maximum number of coefficients contained in the cross-section library, if $<3$). The defaults $S_8/P_3$ should be a good choice for many applications, but the user is free to change them. For transport within complex ducts or over a large distance at small angles, $S_{12}$ may be required. Values of $S_4/P_1$ or even $S_2/P_0$ would be useful in doing a very cursory run just to check whether the problem was input correctly.

In problems with small sources or media that are not highly scattering, discrete ordinates calculations can suffer from "ray effects"—effects in which artifacts of the quadrature directions can be seen in the computed fluxes. To help alleviate the ray effects problem, Denovo has a first collision capability. This computes the amount of uncollided flux in each mesh cell from a point source. These uncollided fluxes are then used as a distributed source in the main discrete ordinates solution. At the end of the main calculation, the uncollided fluxes are added to the fluxes computed after the first collision, forming the total flux. Although this method helps reduce ray effects in many problems, the first collision calculation can require a long computation time for a mesh with many cells or for many point sources.

Adjoint sources in MAVRIC that use point locations will automatically use the Denovo first collision estimation capability. Volumetric adjoint sources will be treated without the first collision capability. It should also be noted that Denovo is a fixed-source $S_N$ solver and cannot model multiplying media. Calculations from Denovo will not be accurate when neutron multiplication is a major source component. By default, MAVRIC instructs Denovo not to perform outer iterations for neutron problems if the cross-section library contains upscatter groups. This is because the time required to calculate the fluxes using upscatter can be significantly longer than the time not using it. For problems in which thermal neutrons are an important part of the transport or tallies, the user can specify that the upscatter iterations be performed in Denovo. This will give more accurate results but requires a longer time for the discrete ordinates calculation.

MAVRIC can be run in separate steps, allowing the user to start a Monaco calculation with previously calculated importance maps or biased sources. Runs can also start with precomputed adjoint fluxes. In this case, the importance map and biased source will be constructed and then passed along to the Monaco Monte Carlo calculation.

### III.B. Example: Dose Rates from a Simplified Cask Model

MAVRIC is best demonstrated by using an example. As an example, consider calculating the neutron dose rate at six locations outside a spent-fuel storage cask.

#### *III.B.1. Problem Description*

For this example, a simplified cask model will be used. The full-size cylindrical cask model consists of an inner steel liner, a thick section of concrete, and an outer steel cover, as shown in Fig. 7. Vent ports at the top and bottom of the cask are modeled as void all of the way around the cask. The interior of the cask is modeled using materials from typical pressurized-water reactor (PWR) fresh fuel assemblies, homogenized over the interior volume. The total mass of the fuel/assembly hardware in this region is 10.6 tonnes. Separate end regions of the assemblies are not modeled in this simple example. Also, note that the fuel material is based on fresh fuel, not spent fuel with its hundreds of fission products. Dose equivalent rates are calculated at six points outside the cask, including in front of the vent port.

Simulated spent fuel from a typical mid-size PWR was used to determine the source term. ORIGEN was used to deplete a full core (46.1 tonnes of uranium, 4.2% enriched, with O, Zr, Fe, Ni, Cr, Sn, and other elements) to 55 000 MWd/tonne U. The contents of the modeled

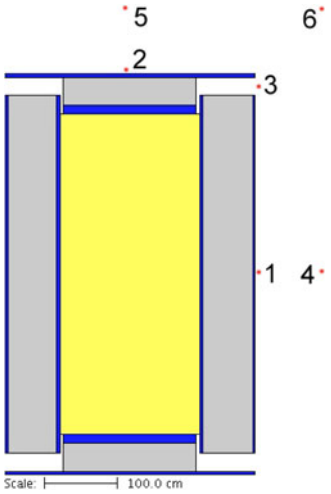


Fig. 7. Vertical slice through the simplified spent fuel cask model, showing the locations of the six detectors.

fuel represent typical values for PWR fuel. ORIGEN then computed the neutron spectra in the 27-group energy structure for the fuel following a 10-yr cooling period after the last irradiation. The total neutron source strength for the cask (1/6 of a full core—about 20 assemblies) was $8.576 \times 10^9$ n/s. The source spectrum and neutron dose response function are shown in Figs. 8 and 9. Calculations in this example all used the ENDF/B-VII.0 cross-section library.

### *III.B.2. Analog Calculations*

A calculation without variance reduction (using only implicit capture) was run for 86 h. Results for the dose rates at each of the six detector locations are listed in Table II. Note that even after 86 h, some of the relative uncertainties in the point detector tallies are at or above

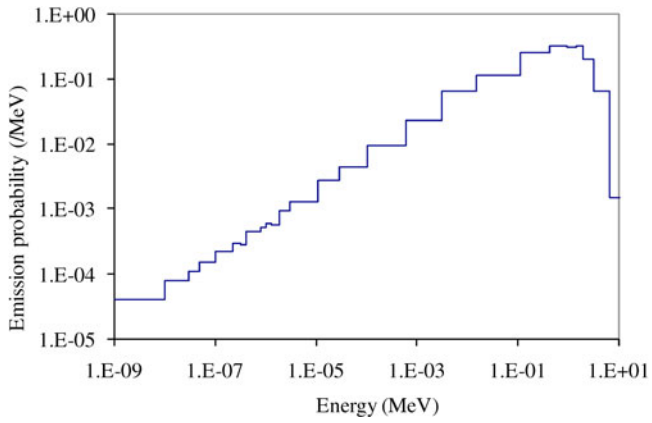


Fig. 8. Spent fuel neutron source spectrum, with strength $8.576 \times 10^9$/s.

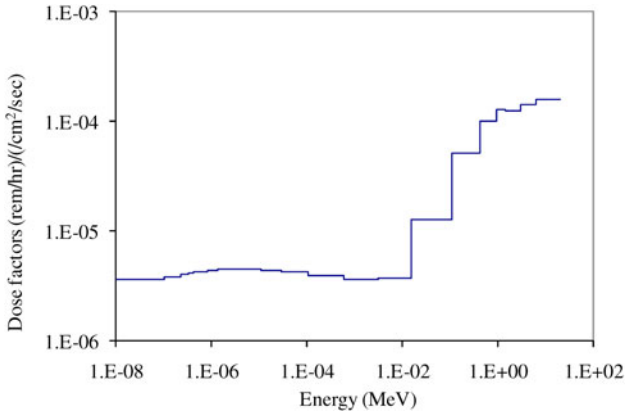


Fig. 9. ANSI standard neutron flux-to-dose conversion factors $(\text{rem/h})/(\text{n/cm}^2 \cdot \text{s}^{-1})$.

TABLE II

Analog Monaco Dose Rate Results for the Simplified Cask Model

| Detector | Dose Rate (rem/h) | Relative Uncertainty |
|---|---|---|
| 1 | 5.54E−04[a] | 0.2401 |
| 2 | 6.97E−03 | 0.0590 |
| 3 | 1.55E−02 | 0.0202 |
| 4 | 4.57E−04 | 0.0470 |
| 5 | 1.36E−02 | 0.0091 |
| 6 | 2.91E−03 | 0.0116 |

[a]Read as $5.54 \times 10^{-4}$.

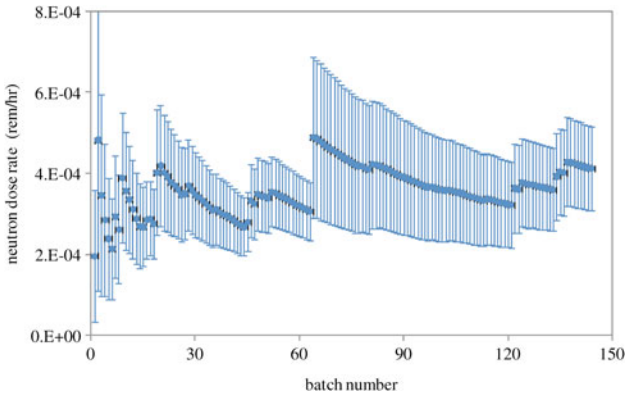


Fig. 10. Convergence plot for the neutron dose rate at point detector 1. Error bars show the $1\sigma$ tally uncertainties.

5%. Figure 10 shows the convergence plot for the neutron dose rate at point detector 1, showing that the tally is not well converged and that some batches contain rare events that change the tally value significantly.

TABLE III

SAS4 Dose Rate Results, Using Radial Biasing and Axial Biasing

| Detector | Radial Biasing | | Axial Biasing | |
|---|---|---|---|---|
| | Dose Rate (rem/h) | Relative Uncertainty | Dose Rate (rem/h) | Relative Uncertainty |
| 1 | 7.63E−04[a] | 0.0076 | 8.98E−05 | 0.6994 |
| 2 | 8.84E−03 | 0.4352 | 7.76E−03 | 0.0039 |
| 3 | 1.41E−02 | 0.1322 | 1.53E−02 | 0.0078 |
| 4 | 4.60E−04 | 0.0099 | 2.91E−04 | 0.5478 |
| 5 | 1.73E−02 | 0.1333 | 1.36E−02 | 0.0049 |
| 6 | 3.49E−03 | 0.1707 | 2.88E−03 | 0.0088 |

[a]Read as $7.63 \times 10^{-4}$.

### *III.B.3. SAS4 Calculations*

Calculations for this problem were also done using the SAS4 sequence in SCALE 5.1. SAS4 was specifically designed for cask geometries and used a one-dimensional discrete ordinates calculation (either radially or axially) to determine weight windows. Results are shown in Table III. Note that SAS4 using radial biasing is expected to perform well only for the two radial point detector locations (1 and 4). Similarly, only the two axial point detectors (2 and 5) are expected to perform well when using axial biasing. SAS4 was not intended to perform well for the points near the vent port (3 and 6), but the results using the axial biasing seem reasonable. Each SAS4 calculation was allowed to run for 6 h.

### *III.B.4. MAVRIC Using CADIS*

In the analog calculations, the dose rates at all six points could be calculated at the same time. With MAVRIC using CADIS, however, the importance map will help keep only the particles moving toward a selected detector location. Thus, each detector will have a separate calculation with an importance map tailored to reduce the variance for just that detector. However, a single calculation will suffice for detector locations that are close together. For example, the importance maps for detectors 1 and 4 both encourage particles that are moving out of the cask in the positive $x$ direction and toward the $z = 0$ plane. In this example, all six detectors will use separate importance maps.

For the importance map, the user lists in the input what planes to use for the adjoint discrete ordinates calculation. These planes define cells, which Denovo treats as homogenous cubes made of a material corresponding to the center point of the cell in the true geometry. Users should select mesh planes that bound as many materials as possible. More mesh planes should be used where the spatial variation of the importance (adjoint flux) is high, for example, near the adjoint sources (the detector positions). It is also important to have planes on the true source bounding box.

In this example problem, different sets of mesh planes will be used for the different detector positions. For detector positions 1 and 4, the mesh planes are shown in Figs. 11 and 12. Note that there are more planes closer to the detectors. Also, note that in the $z$ dimension, it is quite easy to place mesh planes at every material boundary but more difficult to do so in the $x$ and $y$ dimensions because of the curved surfaces. Users need not worry about getting

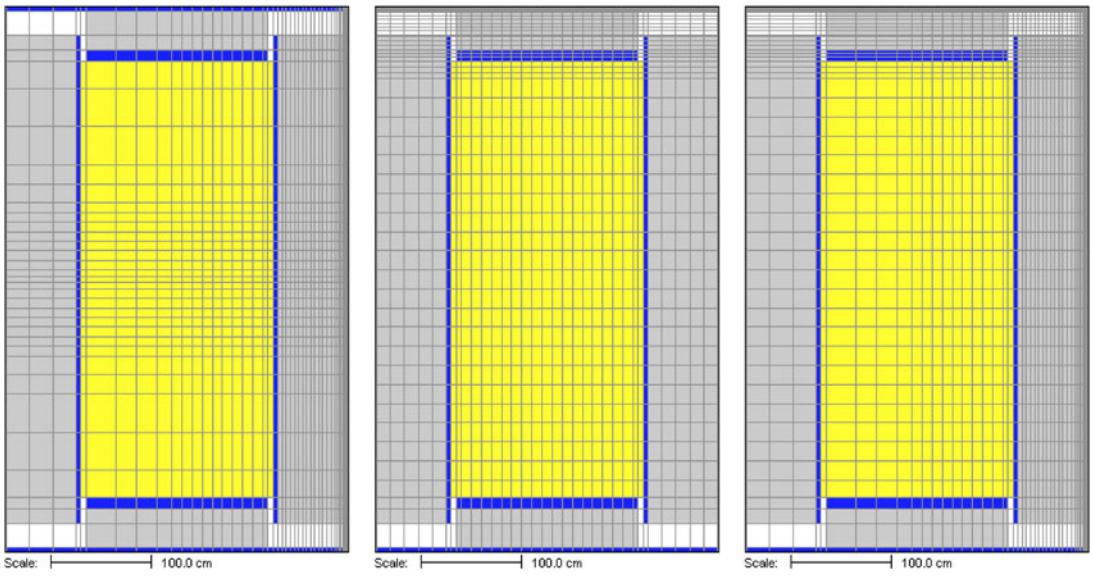


Fig. 11. Importance map mesh planes in the $x$ and $z$ dimensions for detector positions 1/4, 2/5, and 3/6.

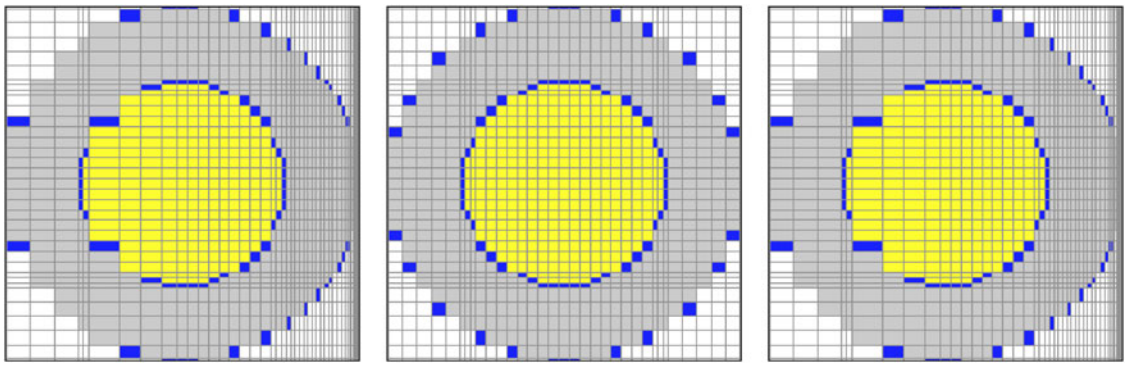

Fig. 12. Importance map mesh planes in the $x$ and $y$ dimensions for detector positions 1/4, 2/5, and 3/6.

things perfect—an approximate importance map can still reduce Monte Carlo variances significantly. The meshes used for detector positions 2/5 and positions 3/6 are also shown in Figs. 11 and 12.

To better illustrate the various steps within the MAVRIC sequence, consider the calculation for the dose rate at detector position 3. First, an adjoint Denovo calculation is done using an adjoint source located at position 3 with an energy spectrum equal to the neutron dose rate flux-to-dose conversion factors. The scalar adjoint fluxes produced by Denovo, which can be viewed using the Java Mesh File Viewer that is shipped with SCALE 6, are shown in Fig. 13 for several of the neutron energy groups.

MAVRIC then combined a mesh representation of the true source (space and energy) with the adjoint fluxes to create the importance map and mesh-based biased source. These are shown in Fig. 14 for the fifth neutron group, covering the energy range of 0.9 to 1.4 MeV. Notice how the most important region (lowest target weights)

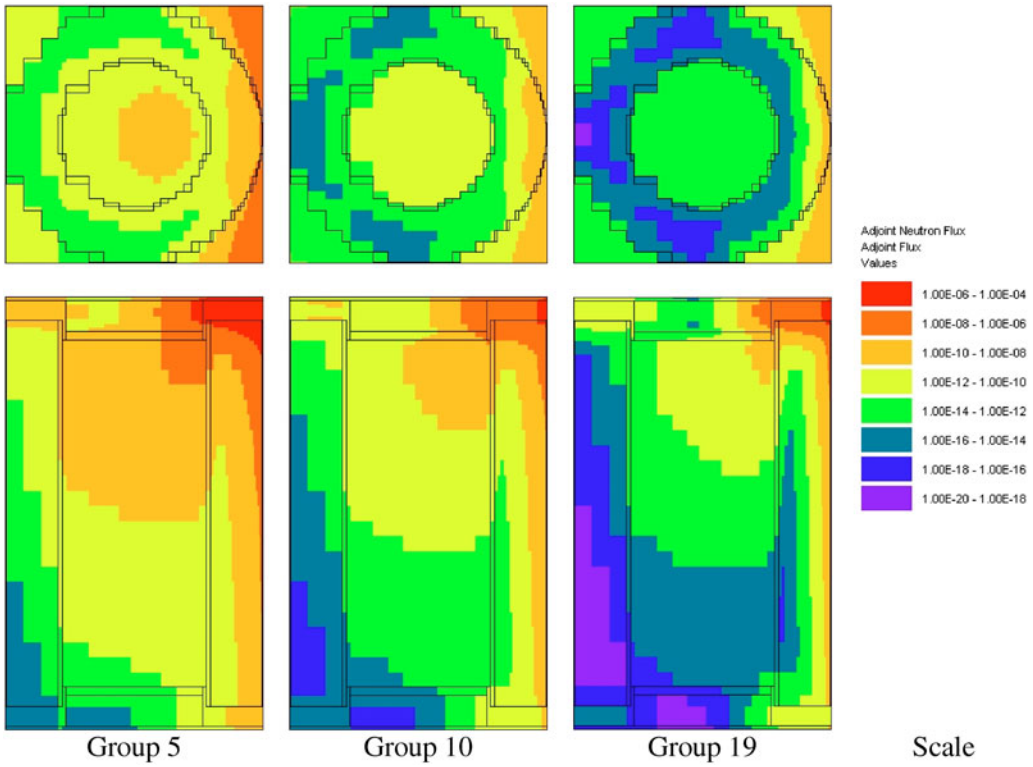


Fig. 13. Adjoint neutron fluxes ($cm^{-2} \cdot s^{-1}$) for groups 5 (0.9 to 1.4 MeV), 10 (0.58 to 3.0 keV), and 19 (0.8 to 1 eV) calculated by Denovo.

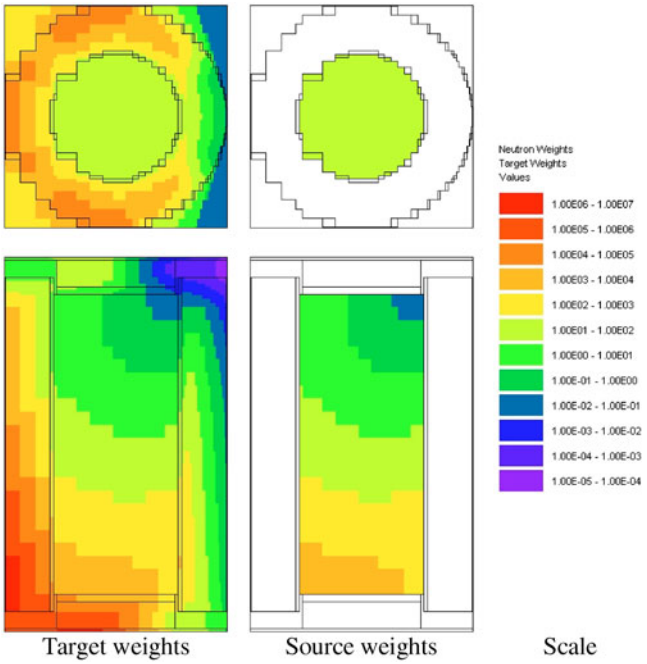


Fig. 14. Neutron target weights from the importance map and source weights (at birth) for neutron group 5 (0.9 to 1.4 MeV).

is adjacent to the vent port near detector position 3. This is something we know qualitatively, but precise quantitative estimates for the variation of importance with space and energy would have been difficult to guess. Also notice the "consistent" part of CADIS—the source particles are born with a weight that matches the target weight for the location in which they are born. The biased source sampling distribution, Fig. 15, shows that the source particles nearest to detector 3 will be sampled more often.

Results for the six MAVRIC calculations, one for each detector, are shown in Table IV. The purpose of this example is to show that MAVRIC, using CADIS, obtains the same answer much more quickly than the analog Monaco calculations. This conclusion can be seen by comparing the MAVRIC results with the results for the analog Monaco and SAS4 calculations, all of which are listed together in Table V.

To account for the time $T$ required to achieve a given relative uncertainty $\sigma$, the calculation figure of merit (FOM) can be determined for each of the codes. The FOM is defined as

$$\text{FOM} = \frac{1}{T\sigma^2} \tag{29}$$

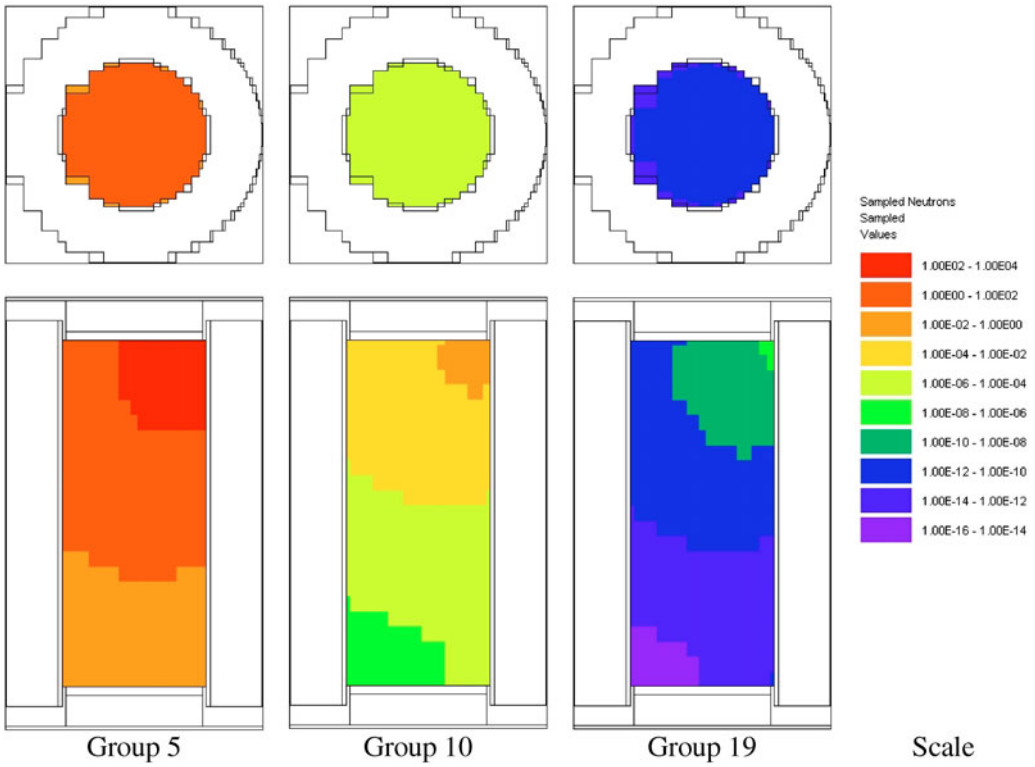


Fig. 15. Biased source sampling probability (n/cm$^3$) for neutron groups 5 (0.9 to 1.4 MeV), 10 (0.58 to 3.0 keV), and 19 (0.8 to 1 eV).

TABLE IV

MAVRIC Dose Rate Results from Six CADIS Calculations

| Detector | Time (min) | | Dose Rate (rem/h) | Relative Uncertainty |
|---|---|---|---|---|
| | Denovo | Monaco | | |
| 1 | 8 | 120 | 7.07E−04[a] | 0.0067 |
| 2 | 9 | 61 | 7.77E−03 | 0.0048 |
| 3 | 12 | 61 | 1.54E−02 | 0.0036 |
| 4 | 8 | 121 | 4.27E−04 | 0.0070 |
| 5 | 9 | 61 | 1.35E−02 | 0.0024 |
| 6 | 12 | 61 | 2.91E−03 | 0.0023 |

[a]Read as $7.07 \times 10^{-4}$.

and measures the efficiency of a Monte Carlo calculation. The ratios of the FOM for each code to the FOM of analog Monaco (speedup) are listed in Table VI to show how much faster MAVRIC and SAS4 are compared with analog Monaco. The FOMs for MAVRIC include the Denovo calculation times. The FOMs for analog Monaco and SAS4 were modified to account for calculating all six detectors simultaneously.

### III.C. MAVRIC Validation

K. Ueki of the Nuclear Technology Division of the Ship Research Institute in Japan performed many simple studies on a variety of shielding materials layered in different combinations.[13] He and his colleagues used both $^{252}$Cf neutron and $^{60}$Co photon sources to investigate the shielding effectiveness of steel, graphite, and many hydrogen-containing materials as single shields or in combination.

One such series of measurements was for pure graphite.[14] A $^{252}$Cf neutron source was placed in the center of a 50-cm cube of paraffin with a 45-deg cone cutout, as shown in Fig. 16. A neutron meter was placed 110 cm

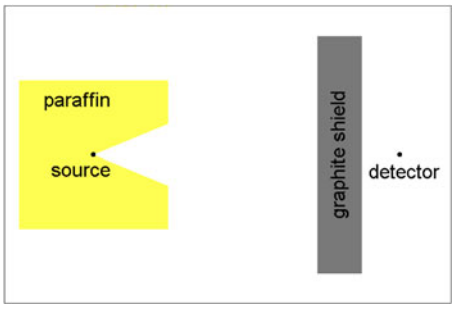


Fig. 16. Example of a two-material Ueki experiment, showing a cutaway view of the paraffin block.

from the source. Sheets of material in $5 \times 80 \times 80$ cm slabs were placed between the source and detector, with the detector side of the shield always fixed at 90 cm from the source. The shield thickness was increased on the source side of the shield. His results (read from a plot) for different thicknesses of graphite are shown in Table VII. Measurement uncertainties were not included with the results.

MAVRIC calculations of the neutron dose attenuation of the graphite slabs were performed using two methods: without variance reduction (Monaco with its standard implicit capture) and with CADIS variance reduction, with the adjoint source at the detector location. The analog Monaco calculations for each shield thickness were run for 1 h, and the MAVRIC/CADIS calculations each required 1 min for the adjoint Denovo calculation and 2 to 10 min for the Monaco Monte Carlo calculation.

The MAVRIC results for each thickness of graphite, listed in Table VIII, show that the MAVRIC results match experiment as well as the analog Monaco values. Relative uncertainties and ratios to the experimental results are also listed in Table VIII. For the 35-cm-thick case, the FOM for the CADIS calculation was about 50 times greater than the FOM for analog Monaco.

TABLE V

Comparison of Calculated Dose Rates*

| Detector | Analog Monaco | SAS4 Radial | SAS4 Axial | MAVRIC |
|---|---|---|---|---|
| | 5164 min | 360 min | 360 min | 543 min |
| 1 | 5.54E−04[a] ± 24.0% | 7.63E−04 ± 0.8% | 8.98E−05 ± 69.9% | 7.07E−04 ± 0.7% |
| 2 | 6.97E−03 ± 5.9% | 8.84E−03 ± 43.5% | 7.76E−03 ± 0.4% | 7.77E−03 ± 0.5% |
| 3 | 1.55E−02 ± 2.0% | 1.41E−02 ± 13.2% | 1.53E−02 ± 0.8% | 1.54E−02 ± 0.4% |
| 4 | 4.57E−04 ± 4.7% | 4.60E−04 ± 1.0% | 2.91E−04 ± 54.8% | 4.27E−04 ± 0.7% |
| 5 | 1.36E−02 ± 0.9% | 1.73E−02 ± 13.3% | 1.36E−02 ± 0.5% | 1.35E−02 ± 0.2% |
| 6 | 2.91E−03 ± 1.2% | 3.49E−03 ± 17.1% | 2.88E−03 ± 0.9% | 2.91E−03 ± 0.2% |

*(rem/h)
[a]Read as $5.54 \times 10^{-4}$.

TABLE VI

Ratio of the Figure of Merit (Speedup) of MAVRIC and SAS4 Compared with Analog Monaco

| Detector | Monaco | SAS4 Radial | SAS4 Axial | MAVRIC |
|---|---|---|---|---|
| 1 | 1 | 14 227 | 1.7 | 8759 |
| 2 | 1 | 0.3 | 3370 | 1880 |
| 3 | 1 | 0.3 | 95 | 372 |
| 4 | 1 | 322 | 0.1 | 298 |
| 5 | 1 | 0.1 | 51 | 176 |
| 6 | 1 | 0.1 | 25.1 | 305 |

TABLE VII

Ueki's Experimental Results for Neutron Attenuation of Graphite Slabs*

| Thickness (cm) | Dose Equivalent Attenuation |
|---|---|
| 2 | 0.8288 |
| 5 | 0.7217 |
| 10 | 0.5261 |
| 15 | 0.3649 |
| 20 | 0.2532 |
| 25 | 0.1705 |
| 30 | 0.1126 |
| 35 | 0.0742 |

*Reference 13.

## IV. OPTIMIZING THE CALCULATION OF MULTIPLE TALLIES

The CADIS methodology works quite well for classical source-detector problems. The statistical uncertainty of the tally that serves as the adjoint source is greatly reduced because the Monte Carlo transport is optimized to spend more simulation time on those particles that contribute to the tally, at the expense of tracking particles in other parts of phase space. But more recently, Monte Carlo has been applied to problems in which multiple tallies all need to be found with low statistical uncertainties. The extension of this idea is the mesh tally, where each voxel is a tally for which low statistical uncertainty is desired. For these problems, the user must accept a total simulation time that is controlled by the tally with the slowest convergence rate or simulation results in which the final tallies have a wide range of relative uncertainties.

The obvious way around this problem is to create a separate problem for each tally and use CADIS to optimize each. Each simulation can then be run until the tally reaches the level of acceptable uncertainty. For more than a few tallies, this approach becomes complicated and time consuming for the user. For mesh tallies, this approach is not reasonable.

Another approach to treating several tallies in close proximity to one another, or a mesh tally covering a small portion of the physical problem, is to use the CADIS methodology with the adjoint source near the middle of the tallies to be optimized. Since particles in the forward Monte Carlo simulation are optimized to reach the location of the adjoint source, all the tallies surrounding that adjoint source should converge quickly. The drawback to this approach is the difficult question of how close the tallies should be. If they are too far apart, certain energies or regions that are needed for one tally may be of low importance for transporting particles to the central adjoint source. As a result, the flux or dose rate at some of the tally sites may be underpredicted.

MAVRIC has the capability to have multiple adjoint sources to address this problem. For several tallies that

TABLE VIII

Comparison of Analog Monaco and MAVRIC Calculations with Experimental Measurements for Attenuation of Neutron Doses Through Slabs of Graphite

| Thickness (cm) | Analog Monaco | | | MAVRIC with CADIS | | |
|---|---|---|---|---|---|---|
| | Attenuation | Relative Uncertainty | Calculated-to-Experiment Ratio | Attenuation | Relative Uncertainty | Calculated-to-Experiment Ratio |
| 2 | 0.8751 | 0.0042 | 1.06 | 0.8728 | 0.0065 | 1.05 |
| 5 | 0.7267 | 0.0065 | 1.01 | 0.7270 | 0.0044 | 1.01 |
| 10 | 0.5312 | 0.0092 | 1.01 | 0.5358 | 0.0054 | 1.02 |
| 15 | 0.3832 | 0.0117 | 1.05 | 0.3761 | 0.0068 | 1.03 |
| 20 | 0.2582 | 0.0145 | 1.02 | 0.2553 | 0.0063 | 1.01 |
| 25 | 0.1754 | 0.0178 | 1.03 | 0.1717 | 0.0067 | 1.01 |
| 30 | 0.1156 | 0.0214 | 1.03 | 0.1121 | 0.0077 | 1.00 |
| 35 | 0.0741 | 0.0269 | 1.00 | 0.0731 | 0.0087 | 0.99 |

are far from each other, multiple adjoint sources can be used. In the forward Monte Carlo, particles would be drawn to one of those adjoint sources. The difficulty with this approach is that typically the tally that is closest to the true physical source converges faster than the other tallies, showing that the closest adjoint source seems to attract more particles than the others. Assigning more adjoint source strength to the farther tallies helps, but finding the correct strengths so that all of the tallies converge to the same relative uncertainty in one simulation is an iterative process for the user.

To converge several tallies to the same relative uncertainty in the one simulation, the adjoint source corresponding to each of those tallies needs to be weighted inversely by the expected tally value. To calculate the dose rate at two points—one near a reactor and one far from a reactor—in one simulation, the total adjoint source used to develop the weight windows and biased source needs to have two parts. The adjoint source far from the reactor needs to have more strength than the adjoint source near the reactor by a factor equal to the ratio of the expected near dose rate to the expected far dose rate.

This concept can be extended to mesh tallies as well. Instead of using a uniform adjoint source strength over the entire mesh tally volume, each voxel of the adjoint source should be weighted inversely by the expected forward tally value for that voxel. Areas of low flux or low dose rate would have more adjoint source strength than areas of high flux or high dose rate. An estimate of the expected tally results can be found by using a coarse-mesh discrete ordinates code. This leads to an extension of the CADIS method called forward-weighted CADIS (FW-CADIS), since the source for the adjoint calculation has been weighted by the forward response.[15–18]

### IV.A. Methods/Implementation

First, a forward $S_N$ calculation is done to estimate the expected tally results. A total adjoint source is constructed where the adjoint source corresponding to each tally is weighted inversely by those forward tally estimates. Then, the standard CADIS approach is used—an importance map (target weight windows) and a biased source are made using the adjoint flux computed from the adjoint $S_N$ calculation.

For example, if the goal is to calculate a detector response function $\sigma_d(\vec{r}, E)$ (such as dose rate using flux-to-dose conversion factors) over a mesh tally, then instead of $q^+(\vec{r}, E) = \sigma_d(\vec{r}, E)$, the adjoint source would be

$$q^+(\vec{r}, E) = \frac{\sigma_d(\vec{r}, E)}{\int \phi(\vec{r}, E)\,\sigma_d(\vec{r}, E)\,dE} \quad , \tag{30}$$

where $\phi(\vec{r}, E)$ is an estimate of the forward flux and the integral is over the voxel at $\vec{r}$. The adjoint source is nonzero only where the mesh tally is defined, and the adjoint source strength is inversely proportional to the forward estimate of dose rate.

The relative uncertainty of a tally is controlled by two things: the number of tracks contributing to the tally and the shape of the distribution of scores contributing to that tally. In the Monte Carlo game, the number of simulated particles $m(\vec{r}, E)$ can be related to the true physical particle density $n(\vec{r}, E)$ by the average Monte Carlo weight of scoring particles $\overline{w}(\vec{r}, E)$ by

$$n(\vec{r}, E) = \overline{w}(\vec{r}, E) m(\vec{r}, E) \quad . \tag{31}$$

In a typical Monte Carlo calculation, tallies are made by adding some score, multiplied by the current particle weight, to an accumulator. To calculate a similar quantity related to the Monte Carlo particle density would be very close to calculating any other quantity but without including the particle weight. The goal of FW-CADIS is to make the Monte Carlo particle density $m(\vec{r}, E)$ more uniform over the tally areas. So, an importance map needs to be developed that represents the importance necessary for achieving uniform Monte Carlo particle density. In the attempt to keep the Monte Carlo particle density more uniform, more uniform relative errors for the tallies will be realized.

To optimize the forward Monte Carlo simulation for the calculation of some quantity at multiple tally locations or across a mesh tally, the adjoint source needs to be weighted by the estimate of that quantity. Three "flavors" are offered in MAVRIC as shown in Table IX.

The bottom line of FW-CADIS is that in order to calculate a quantity at multiple tally locations (or across a mesh tally) with nearly uniform relative uncertainties, an adjoint source needs to be developed that keeps the Monte Carlo particle density constant. FW-CADIS uses a forward discrete ordinates calculation to form the adjoint source that transports more particles to low-flux areas of phase space. After that, the standard CADIS approach is used.

It should be noted that hybrid methods developed by Cooper and Larsen[19] and Becker and Larsen[20] use only an estimate of the forward fluxes to construct weight windows that distribute Monte Carlo particles uniformly in space and energy. These methods are designed for solving "global" problems—low relative uncertainties in every mesh and at every energy group in the entire problem.

### IV.B. Example: Dose Rates from a Simplified Cask Model

The FW-CADIS method can be demonstrated with a continuation of the example used in Sec. III.B for calculating the neutron dose rates outside a simplified spent-fuel storage cask. For comparison, a calculation can be done with adjoint sources placed at all six detector locations and equally weighted. Dose rate results for such a calculation are given in Table X and show that the areas of higher dose rate have lower relative uncertainties. These

TABLE IX

Adjoint Sources for Different Types of Forward Weighting

| For the Calculation of | | Use an Adjoint Source of |
|---|---|---|
| Energy and spatially dependent flux | $\phi(\vec{r},E)$ | $q^+(\vec{r},E)=\frac{1}{\phi(\vec{r},E)}$ |
| Spatially dependent total flux | $\int \phi(\vec{r},E)\,dE$ | $q^+(\vec{r},E)=\frac{1}{\int \phi(\vec{r},E)\,dE}$ |
| Spatially dependent total dose rate | $\int \phi(\vec{r},E)\sigma_d(\vec{r},E)\,dE$ | $q^+(\vec{r},E)=\frac{\sigma_d(\vec{r},E)}{\int \phi(\vec{r},E)\sigma_d(\vec{r},E)\,dE}$ |

TABLE X

CADIS Dose Rate Results with Six Adjoint Sources Equally Weighted

| Detector | Dose Rate (rem/h) |
|---|---|
| 1 | 7.48E−04[a] ± 6.3% |
| 2 | 7.77E−03 ± 0.6% |
| 3 | 1.55E−02 ± 1.1% |
| 4 | 4.26E−04 ± 2.4% |
| 5 | 1.35E−02 ± 0.5% |
| 6 | 2.91E−03 ± 0.4% |

[a]Read as $7.48 \times 10^{-4}$.

TABLE XI

Neutron Dose Rate Estimates and Normalized Adjoint Source Strengths

| Detector | Dose Rate (rem/h) | Adjoint Source Strength |
|---|---|---|
| 1 | 7.93E−04[a] | 0.3845 |
| 2 | 1.20E−02 | 0.0254 |
| 3 | 1.54E−02 | 0.0198 |
| 4 | 6.87E−04 | 0.4438 |
| 5 | 1.30E−02 | 0.0234 |
| 6 | 2.96E−03 | 0.1031 |

[a]Read as $7.93 \times 10^{-4}$.

results are for a MAVRIC run consisting of a 26-min adjoint Denovo calculation and a 124-min Monaco calculation.

A MAVRIC calculation with forward weighting adjusts the strengths of the adjoint source in order to achieve a more uniform Monte Carlo particle density at each tally location. Using FW-CADIS in MAVRIC requires only two more keywords in the user input file. The first step in MAVRIC is to perform a forward discrete ordinates calculation with Denovo to estimate the forward flux and dose rates at the tally locations. The adjoint source is made by taking each of the six adjoint sources and dividing the strength (default = 1) by the estimate of the dose rate at those locations. The dose rate estimates and adjoint source strengths are listed in Table XI. The Denovo calculated forward fluxes and dose rates are shown in Figs. 17 and 18.

The CADIS method then proceeds as normal—the adjoint calculation is done by Denovo; the importance map and biased source are computed and passed to Monaco for the forward Monte Carlo calculation. The importance map and biased source are shown in Fig. 19. The final results of the MAVRIC FW-CADIS calculation are shown in Table XII. Since the adjoint sources were weighted, comparable numbers of Monte Carlo particles got to the detectors in the low dose rate areas and in the high dose rate areas, giving more uniform relative uncertainties. For this problem, the forward Denovo calculation

TABLE XII

FW-CADIS Dose Rate Results

| Detector | Dose Rate (rem/h) |
|---|---|
| 1 | 6.99E−04[a] ± 1.1% |
| 2 | 7.77E−03 ± 0.7% |
| 3 | 1.53E−02 ± 0.6% |
| 4 | 4.18E−04 ± 1.0% |
| 5 | 1.35E−02 ± 0.5% |
| 6 | 2.92E−03 ± 0.4% |

[a]Read as $6.99 \times 10^{-4}$.

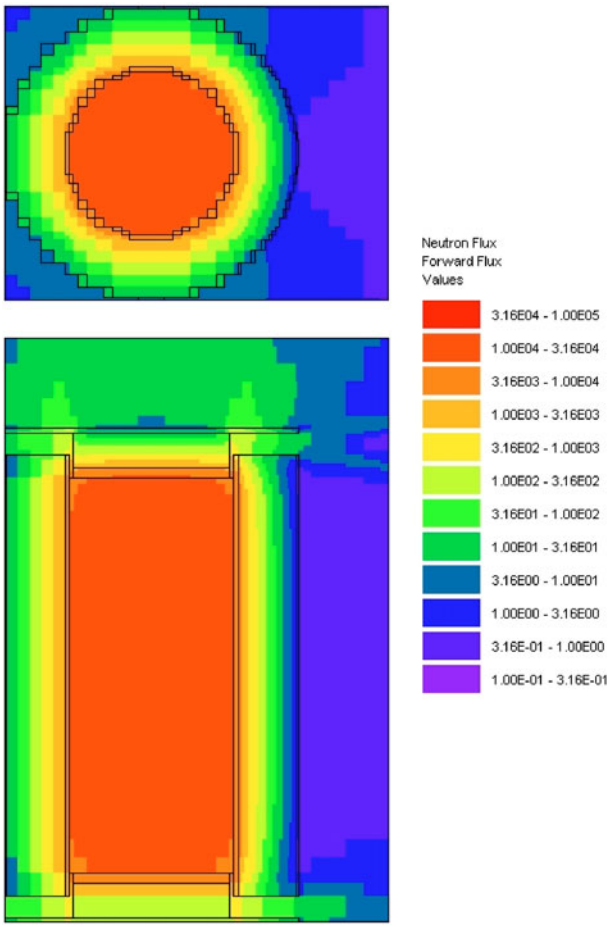


Fig. 17. The group 5 (0.9 to 1.4 MeV) flux ($n/cm^2 \cdot s^{-1}$) from Denovo.

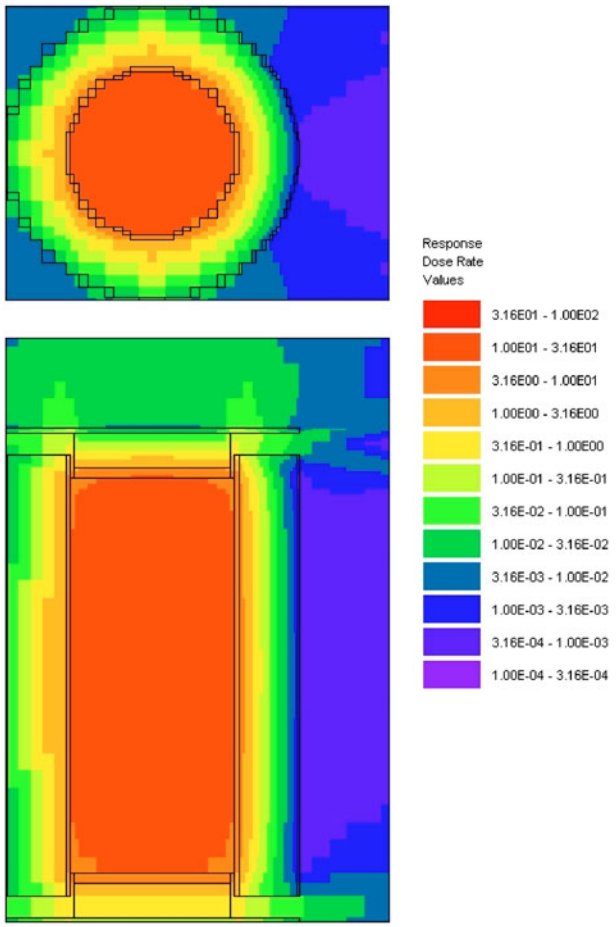


Fig. 18. The total dose rate (rem/h) found by integrating the Denovo fluxes with the response function.

took 20 min, the adjoint Denovo calculation took 25 min, and the forward Monaco calculation took 123 min.

Comparing Tables X and XII, the dose rates for each detector location are the same (within the statistical uncertainty), but the relative uncertainties of the forward-weighted calculation do not vary as much as the relative uncertainties of the calculation without the forward weighting.

An important point about using FW-CADIS is that in order for the flux or dose rate to be estimated by the forward Denovo calculation, the detector locations must be included in the discrete ordinates mesh. Preferably, their locations should be at the centers of the mesh voxels instead of on the mesh planes. If the adjoint sources are not within the discrete ordinates mesh (which is allowed for standard CADIS), then the forward flux or dose rate cannot be found at those locations and a weighting factor of 1 will be used for each. Warning messages are printed to the screen and to the output file if adjoint sources are not located within the discrete ordinates grid.

### IV.C. Example: Total Dose Rates Outside a Cask

For an example with more realism, consider the cask model for the TN-24P, as used in previous SCALE shielding reports[4,21] and shown in Fig. 20. This model contains two types of PWR spent-fuel assemblies (Types V and W, both Westinghouse $15 \times 15$ assemblies of different starting enrichments and burnups), each with specified neutron and photon sources, in an aluminum/boron fuel basket. The cask is made of forged steel for photon shielding with a resin layer for neutron shielding. Also included in the model are three activated hardware regions (bottom nozzle, top nozzle, and top plenum) that consist of specified amounts of $^{60}Co$ (a photon source). The task for this example is to calculate the total dose rate within 2 m of the cask surface.

For MAVRIC, this means the calculation of a dose rate mesh tally using FW-CADIS to ensure that each voxel has low relative uncertainty, independent of the dose rate. Without MAVRIC, the calculation of dose rate everywhere in three dimensions would be too challenging.

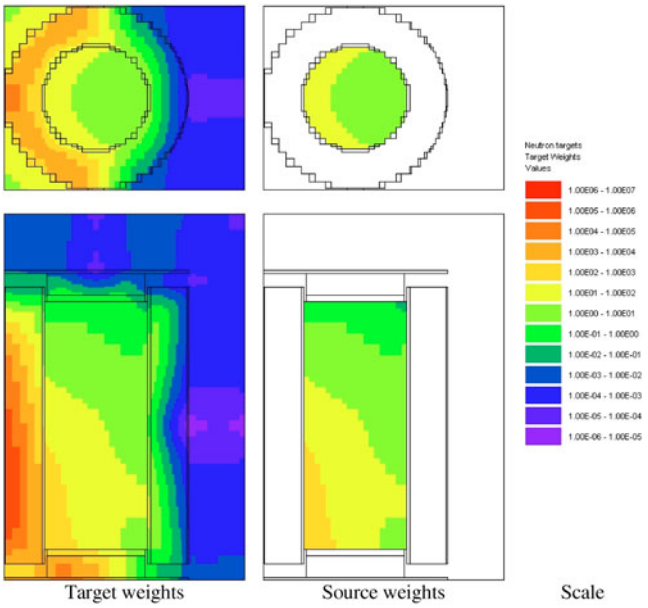


Fig. 19. Importance map (target weights) and the biased source weights from the neutron FW-CADIS method.

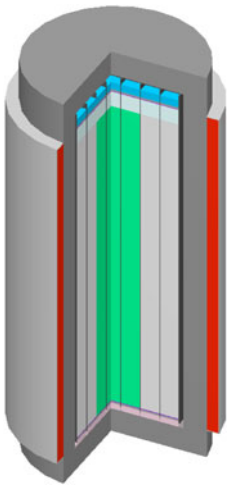

Fig. 20. Model of the TN-24P spent-fuel storage cask.

Most likely, the dose rate would be evaluated with reasonable uncertainty at only a few locations. In fact, with analog calculations, this example would be a very difficult problem since most source particles never leave the cask, just as in the real-life situation. This type of problem really benefits from the CADIS biased source distribution, in which source particles deep inside the cask are sampled very rarely since they do not contribute significantly to the response.

Currently, Monaco can sample only one source description. The cask problem discussed here could be done with five FW-CADIS calculations, each with one source: assembly type V (neutron and photon together), assembly type W (neutron and photon), bottom nozzle, top nozzle, and top plenum. Each would be optimized to calculate the total dose rate (neutron and photon) over a volume extending outward from the cask for 2 m in each direction. However, when neutron and photon sources are combined and optimized on total dose rate, the separate neutron dose and photon dose rates will not be calculated with the same relative uncertainty, if they are not nearly equal in their contributions to total dose rate. If only the total dose rate were needed and the different components of dose rate were not, then this approach would be adequate.

For this example, nine FW-CADIS calculations were used to completely separate out the different components of dose rate from the different sources. These are listed in Table XIII. Each calculation used Denovo to estimate the

TABLE XIII

Nine FW-CADIS Calculations for Separate Dose Rates from Seven Sources

| Source | | Dose Tally | Calculation Time (min) | | | | |
|---|---|---|---|---|---|---|---|
| | | | Forward Denovo | Adjoint Denovo | Source Preparation | Monaco | Total |
| Bottom nozzle | Photon | Photon | 8 | 7 | 0.3 | 364 | 380 |
| Top plenum | Photon | Photon | 9 | 7 | 0.3 | 362 | 379 |
| Top nozzle | Photon | Photon | 9 | 7 | 0.3 | 364 | 381 |
| V assemblies | Neutron | Neutron | 58 | 29 | 48 | 283 | 418 |
| V assemblies | Neutron | Photon | 56 | 56 | 48 | 362 | 523 |
| V assemblies | Photon | Photon | 16 | 13 | 48 | 361 | 438 |
| W assemblies | Neutron | Neutron | 57 | 30 | 21 | 361 | 469 |
| W assemblies | Neutron | Photon | 56 | 57 | 21 | 363 | 497 |
| W assemblies | Photon | Photon | 16 | 13 | 21 | 365 | 414 |

forward fluxes, then solved an adjoint Denovo using a volumetric adjoint source all around the cask weighted inversely by the forward dose rate, then created the importance map and biased source, and finally called Monaco. For this problem, the sources in the spent-fuel assemblies had a nonuniform axial distribution that became very small near the ends. To properly convert this distribution into a mesh-based source for the CADIS routines, many source positions had to be sampled, leading to longer than usual source preparation times. Calculation times are also listed in Table XIII. Vertical slices showing the nine components of dose rate are shown in Fig. 21, and the total dose rate is shown in Fig. 22. The asymmetry seen in the V assembly photon source/photon dose image in Fig. 21 is due to the loading pattern of the spent fuel.

Note that nonuniform spatial distributions are not currently part of the SCALE 6 Monaco/MAVRIC but

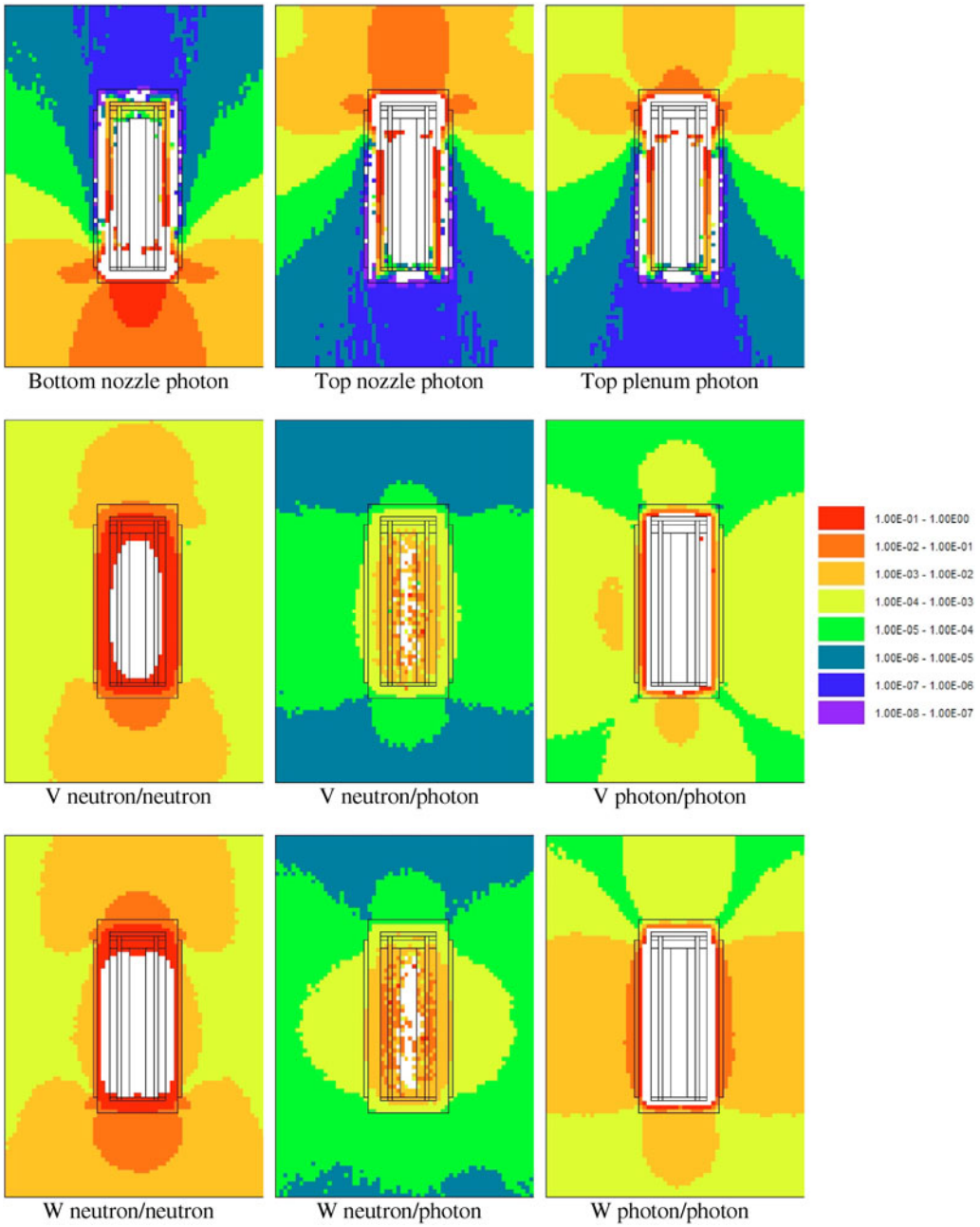


Fig. 21. Nine components of total dose rate (rem/h). Dose rates above 1 rem/h occurred only inside the cask and were not included in the scale.

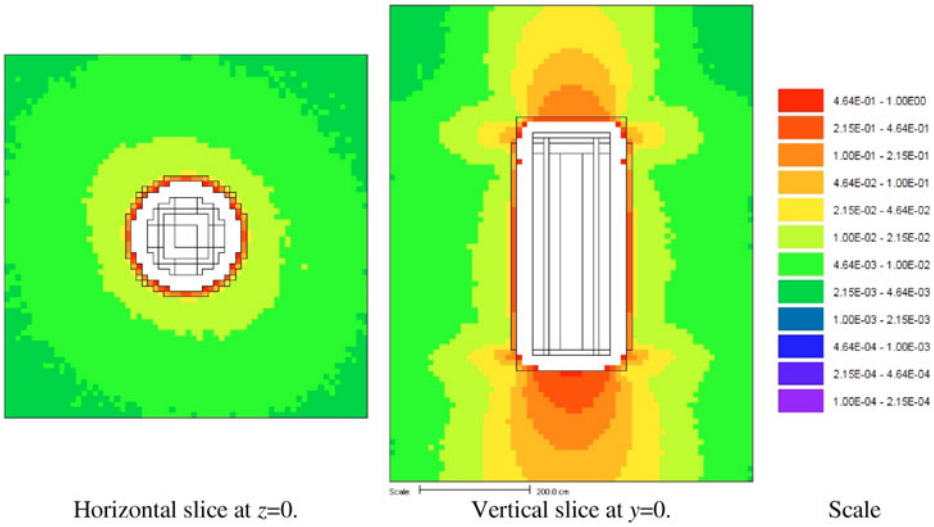


Fig. 22. Total dose rate (both neutron and photon, in rem/h) from seven sources. Dose rates above 1 rem/h occurred only inside the cask and were not included in the scale.

will be available in the next release. Also planned for the next release is the capability to list multiple sources in the MAVRIC input. With this feature, the calculation to find the mesh tally of total dose rate will be achievable with one FW-CADIS calculation, assuming that the details of dose rates from the individual source components are not important. In fact, the importance map and biased source would determine which parts of the source and transport phase space are the most important to the total dose everywhere and focus the Monte Carlo time in those areas.

### IV.D. MAVRIC Validation

A benchmark for measuring neutron dose responses through a three-section concrete labyrinth[22] was simulated using MAVRIC. This benchmark was based on a series of 1982 Russian experimental measurements of the neutron flux from a $^{252}$Cf through an 18-m concrete labyrinth. Six different labyrinths were constructed that ranged from an empty concrete labyrinth, shown in Fig. 23, to designs with different corners lined with different absorbers. Two $^{252}$Cf source sources were used, a bare source and a source encased in a polyethylene sphere. Measurements were made with six Bonner spheres [mostly polyethylene with a $^{6}$LiI(Eu) crystal] of different diameters covered with cadmium (and one detector without cadmium) at ten locations within the labyrinth.

Calculations in the benchmark report used MCNP (Ref. 8) and were done in two steps: (a) the determination of the detector response in a free field and (b) the transport of neutrons through the labyrinth, where the computed fluxes at the detector locations were integrated with the response functions found in the first step.

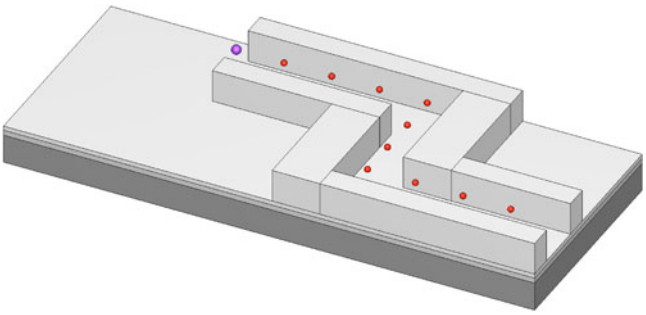

Fig. 23. Geometry of the labyrinth, with roof removed, showing the source position (upper left) and the ten detector locations.

Monaco, MAVRIC, and the new ENDF/B-VII 200n/47g shielding library were used to compute the detector count rates measured by the various detectors for the first labyrinth design (empty, three-section) using both the covered and bare californium source. Calculations followed the benchmark instructions and were done in two steps:

1. Determination of the detector response function using Monaco: For each energy group, a Monaco calculation was done to find the integrated product of the $^{6}\mathrm{Li}(n,t)^{4}\mathrm{He}$ cross section and neutron flux inside the detector crystal. Monaco calculations were done for each energy group (200) incident on each size detector (7).

2. MAVRIC, using the FW-CADIS method, was used to calculate neutron fluxes along the path through the labyrinth. Each FW-CADIS calculation was optimized

for a specific source and response, so calculations had to be done for each source (2) using each detector size (7).

Comparing the Monaco computed detector response functions with the benchmark values of response functions, shown in Figs. 24 and 25, shows that for the larger detector sizes, Monaco predicts a smaller response at lower incident neutron energies than the benchmark MCNP calculations. For the second step, using the benchmark response functions to calculate the detector responses, the values calculated by MAVRIC compared very well with the benchmark values, as shown in Figs. 26 and 27. Both the MAVRIC calculations and the benchmark calculations, in which the responses dropped by over three orders of magnitude from the first detector to the tenth, differ from the measured values. In these figures, the ratio of the computed value to the measured value is shown, and the uncertainties shown are due almost entirely to the uncertainties in the measured values.

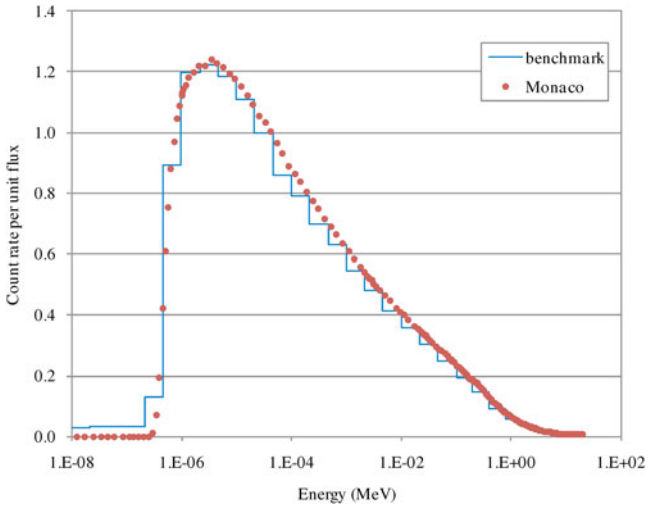


Fig. 24. Response (counts per unit flux) for the 5.1-cm (2-in.)-diam Bonner sphere (with Cd cover).

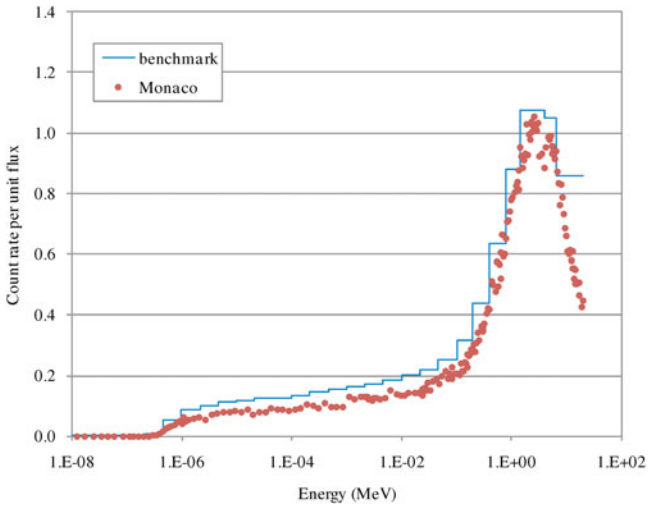


Fig. 25. Response (counts per unit flux) for the 25.4-cm (10-in.)-diam Bonner sphere (with Cd cover).

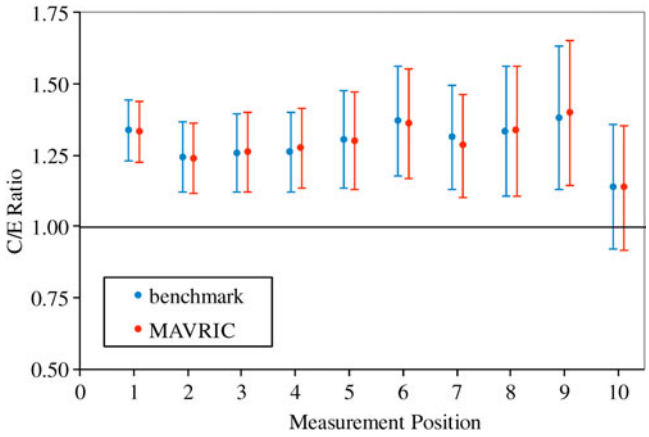


Fig. 26. Neutron count rate calculated-to-experiment ratio for the 5.1-cm (2-in.) Bonner sphere (with Cd cover) and the uncovered $^{252}$Cf source.

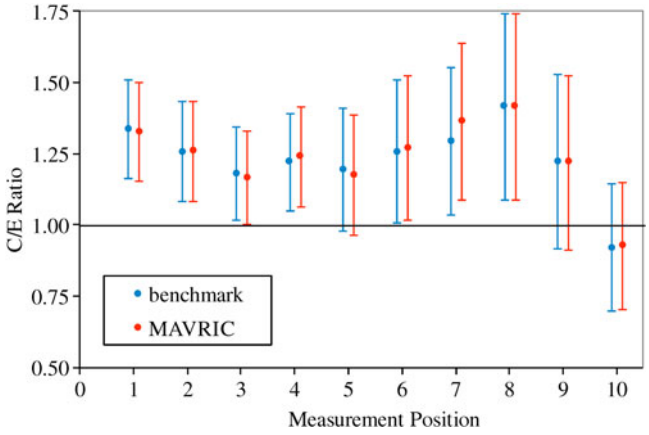


Fig. 27. Neutron count rate calculated-to-experiment ratio for the 25.4-cm (10-in.) Bonner sphere (with Cd cover) and the uncovered $^{252}$Cf source.

## V. SUMMARY

SCALE 6 contains an extensive set of tools to perform a wide variety of 3-D shielding analyses. Basic Monte Carlo transport problems can be solved with Monaco. Deep penetration problems can be solved using the automated variance reduction capabilities of MAVRIC, which utilizes the new Denovo discrete ordinates $S_N$ code.

For the classic source-detector problems, MAVRIC employs the CADIS method to optimize the Monaco simulation for the calculation of a specific detector response. For problems in which responses from multiple detectors or results from a large mesh tally are required, MAVRIC and FW-CADIS can be used to optimize the Monte Carlo calculation so that various tallies are computed with more uniform relative uncertainties. All of these capabilities were demonstrated with several example problems. SCALE 6 also includes Java-based graphical user interface utilities to view the discrete ordinate fluxes, importance maps, biased sources, mesh tallies, and tally convergence data.

## ACKNOWLEDGMENT

Oak Ridge National Laboratory is managed and operated by UT-Battelle, LLC, for the U.S. Department of Energy under contract DE-AC05-00OR22725.

## REFERENCES

1. K. A. VAN RIPER, T. J. URBATSCH, P. D. SORAN, D. K. PARSONS, J. E. MOREL, G. W. McKINNEY, S. R. LEE, L. A. CROTZER, F. W. BRINKLEY, T. E. BOOTH, J. W. ANDERSON, and R. E. ALCOUFFE, "AVATAR—Automatic Variance Reduction in Monte Carlo Calculations," *Proc. Joint. Int. Conf. Mathematical Methods and Supercomputing in Nuclear Applications*, Saratoga Springs, New York, October 6–10, 1997, Vol. 1, p. 661, American Nuclear Society (1997).

2. "SCALE: A Modular Code System for Performing Standardized Computer Analyses for Licensing Evaluation," ORNL/TM-2005/39, Version 5, Vols. I, II, and III (Apr. 2005); see also CCC-725, Radiation Safety Information Computational Center, Oak Ridge National Laboratory.

3. J. C. WAGNER, "Acceleration of Monte Carlo Shielding Calculations with an Automated Variance Reduction Technique and Parallel Processing," PhD Dissertation, The Pennsylvania State University (1997).

4. D. WIARDA, M. E. DUNN, D. E. PEPLOW, T. M. MILLER, and H. AKKURT, "Development and Testing of ENDF/B-VI.8 and ENDF/B-VII.0 Coupled Neutron-Gamma Libraries for SCALE 6," NUREG/CR-6990 (ORNL/TM-2008/047), Nuclear Regulatory Commission, Oak Ridge National Laboratory (Feb. 2009).

5. E. SAJO, M. L. WILLIAMS, and M. ASGARI, "Comparison of Measured and Calculated Neutron Transmission Through Steel for a $^{252}$Cf Source," *Ann. Nucl. Energy*, **20**, 585 (1993).

6. B. JANSKY, Z. TURIK, E. NOVAK, J. KYNCL, F. CVACHOVEC, and P. TILLER, "Comparison of Measured and Calculated Neutron Transmission Through Heavy Water for $^{252}$Cf Source Placed in the Center of 30 cm Diameter Sphere," *Ann. Nucl. Energy*, **24**, 1189 (1997).

7. G. MANTUROV, Y. ROZHIKHIN, and L. TRYKOV, "Neutron and Photon Leakage Spectra from Cf-252 Source at Centers of Six Iron Spheres of Different Diameters" (ALARM-CF-FE-SHIELD-001), *International Handbook of Evaluated Criticality Safety Benchmark Experiments*, *Volume VIII—Criticality Alarm/Shielding Benchmarks*, NEA/NSC/DOC/(95)03, Organisation for Economic Co-operation and Development, Nuclear Energy Agency (Sep. 2007).

8. X-5 MONTE CARLO TEAM, "MCNP—A General Monte Carlo N-Particle Transport Code, Version 5, Volume I: Overview and Theory," LA-UR-03-1987, Los Alamos National Laboratory (2003).

9. T. M. EVANS, A. S. STAFFORD, R. N. SLAYBAUGH, and K. T. CLARNO, "Denovo: A New Three-Dimensional Parallel Discrete Ordinates Code in SCALE," *Nucl. Technol.*, **171**, 171 (2010).

10. J. C. WAGNER and A. HAGHIGHAT, "Automated Variance Reduction of Monte Carlo Shielding Calculations Using the Discrete Ordinates Adjoint Function," *Nucl. Sci. Eng.*, **128**, 186 (1998).

11. J. C. WAGNER, "An Automated Deterministic Variance Reduction Generator for Monte Carlo Shielding Applications," *Proc. 12th Biennial Radiation Protection and Shielding Division Topl. Mtg.*, Santa Fe, New Mexico, April 14–18, 2002, American Nuclear Society (2002).

12. A. HAGHIGHAT and J. C. WAGNER, "Monte Carlo Variance Reduction with Deterministic Importance Functions," *Prog. Nucl. Energy*, **42**, 25 (2003).

13. K. UEKI, A. OHASHI, N. NARIYAMA, S. NAGAYAMA, T. FUJITA, K. HATTORI, and Y. ANAYAMA, "Systematic Evaluation of Neutron Shielding Effects for Materials," *Nucl. Sci. Eng.*, **124**, 455 (1996).

14. K. UEKI, A. OHASHI, and Y. ANAYAMA, "Neutron Shielding Ability of KRAFTON N2–Mannan–KRAFTON N2 Sandwich-Type Material and Others," *Proc. Radiation Protection and Shielding Division Topl. Mtg.*, Pasco, Washington, American Nuclear Society (1992).

15. J. C. WAGNER, E. D. BLAKEMAN, and D. E. PEPLOW, "Forward-Weighted CADIS Method for Global Variance Reduction," *Trans. Am. Nucl. Soc.*, **97**, 630 (2007).

16. D. E. PEPLOW, E. D. BLAKEMAN, and J. C. WAGNER, "Advanced Variance Reduction Strategies for Optimizing Mesh Tallies in MAVRIC," *Trans. Am. Nucl. Soc.*, **97**, 595 (2007).

17. D. E. PEPLOW, T. M. EVANS, and J. C. WAGNER, "Simultaneous Optimization of Tallies in Difficult Shielding Problems," *Nucl. Technol.*, **168**, 785 (2009).

18. J. C. WAGNER, D. E. PEPLOW, and T. M. EVANS, "Automated Variance Reduction Applied to Nuclear Well-Logging Problems," *Nucl. Technol.*, **168**, 799 (2009).

19. M. A. COOPER and E. W. LARSEN, "Automated Weight Windows for Global Monte Carlo Particle Transport Calculations," *Nucl. Sci. Eng.*, **137**, 1 (2001).

20. T. L. BECKER and E. W. LARSEN, "The Application of Weight Windows to "Global" Monte Carlo Problems," *Proc. Int. Conf. Advances in Mathematics, Computational Methods, and Reactor Physics (M&C2009)*, Saratoga Springs, New York, May 3–7, 2009, American Nuclear Society (2009).

21. B. L. BROADHEAD, J. S. TANG, R. L. CHILDS, C. V. PARKS, and H. TANIUCHI, "Evaluation of Shielding Analysis Methods in Spent Fuel Cask Environments," EPRI TR-104329, Electric Power Research Institute (May 1995).

22. M. NIKOLAEV, N. PROKHOROVA, and T. IVANOVA, "Neutron Fields in Three-Section Concrete Labyrinth from Cf-252 Source" (ALARM-CF-AIR-LAB-001), *International Handbook of Evaluated Criticality Safety Benchmark Experiments, Volume VIII—Criticality Alarm/Shielding Benchmarks*, NEA/NSC/DOC/(95)03, Organisation for Economic Co-operation and Development, Nuclear Energy Agency (Sep. 2007).